ACS Catalysis

Review

Cite This: ACS Catal. 2019, 9, 345−364

pubs.acs.org/acscatalysis

Photocatalysis with Reduced TiO_2: From Black TiO_2 to Cocatalyst-Free Hydrogen Production

Alberto Naldoni,*[,†] Marco Altomare,[‡] Giorgio Zoppellaro,[†] Ning Liu,[‡] Štěpán Kment,[†] Radek Zbořil,[†] and Patrik Schmuki*[,†,‡]

[†]Regional Centre of Advanced Technologies and Materials, Faculty of Science, Palacký University Olomouc, Šlechtitelů 27, 78371 Olomouc, Czech Republic

[‡]Department of Materials Science and Engineering, University of Erlangen-Nuremberg, Martensstrasse 7, D-91058 Erlangen, Germany

ABSTRACT: Black TiO_2 nanomaterials have recently emerged as promising candidates for solar-driven photocatalytic hydrogen production. Despite the great efforts to synthesize highly reduced TiO_2, it is apparent that intermediate degree of reduction (namely, gray titania) brings about the formation of peculiar defective catalytic sites enabling cocatalyst-free hydrogen generation. A precise understanding of the structural and electronic nature of these catalytically active sites is still elusive, as well as the fundamental structure−activity relationships that govern formation of crystal defects, increased light absorption, charge separation, and photocatalytic activity. In this Review, we discuss the basic concepts that underlie an effective design of reduced TiO_2 photocatalysts for hydrogen production such as (i) defects formation in reduced TiO_2, (ii) analysis of structure deformation and presence of unpaired electrons through electron paramagnetic resonance spectroscopy, (iii) insights from surface science on electronic singularities due to defects, and (iv) the key differences between black and gray titania, that is, photocatalysts that require Pt-modification and cocatalyst-free photocatalytic hydrogen generation. Finally, future directions to improve the performance of reduced TiO_2 photocatalysts are outlined.

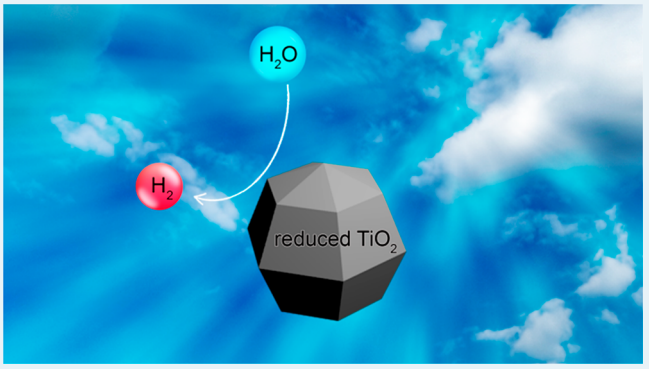

KEYWORDS: *black TiO_2, H_2 production, photocatalysis, hydrogenation, cocatalyst, defect engineering, water splitting*

1. INTRODUCTION

Solar energy storage in the form of chemical bonds is of paramount relevance in the modern energy economy to increase the share of renewable energy utilization at zero-carbon emission.

The ideal energy vector envisioned to store solar energy is molecular H_2. It has high energy density and can be obtained from water splitting, a very well-known chemical reaction that has inspired the development of several technologies such as electrolyzers, photoelectrochemical (PEC) cells, and photocatalytic reactors for powdered catalysts in aqueous suspensions.[1−7]

In particular, photocatalysis with powdered semiconductor catalysts has been greatly developed in the last 50 years finding application in pollutants removal,[8−10] CO_2 photoreduction,[11,12] N_2 fixation,[13] and indeed in H_2 production from water splitting or photoreforming of H_2O/alcohol (i.e., methanol and ethanol) mixtures.[14]

Photocatalytic chemical transformations consist of several consecutive steps, thus limiting the overall photoconversion efficiency. A typical photocatalytic process starts with the generation of electron−hole pairs in the semiconductor bulk following light irradiation, and their subsequent migration toward the surface where reaction with molecular substrates occurs.

TiO_2 is the most diffuse photocatalyst providing a set of material properties such as an outstanding stability toward photocorrosion, nontoxicity, low cost, and conduction and valence band edges (CB and VB, respectively) straddling the redox potentials of many sustainable chemical transformations (Figure 1). However, TiO_2 efficiency has been hampered by its wide bandgap of ∼3.2 eV that limits light absorption to the UV region of the solar spectrum (∼4% of the total solar irradiance).

Furthermore, TiO_2 shows high recombination of photogenerated charge carriers. To mitigate this limit, different approaches have been explored for the material's assembly such as engineering of nanocrystals' shape and facets, formation of heterojunctions with other semiconductors, and the deposition of noble metal (Au or Pt) cocatalysts to enhance charge separation through the formation of an interfacial Schottky barrier.[15,16]

Received: October 9, 2018
Revised: November 26, 2018
Published: November 30, 2018

DOI: 10.1021/acscatal.8b04068
ACS Catal. 2019, 9, 345−364

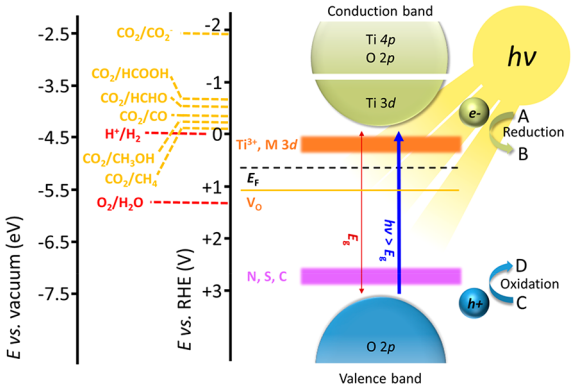

Figure 1. Schematic representation of photocatalysis with TiO_2: red arrow - bandgap energy (E_g) of TiO_2 ~ 3.0−3.2 eV depending on the crystalline structure; blue arrow - photon absorption having energy equal or greater than E_g and consequent excitation of electrons (e^-) to the CB leaving positively charged vacancies, holes (h^+), in the VB. Electrons act as reduction agent, while holes promote oxidation reactions. E_F is the Fermi level of TiO_2. The orange energy states within the TiO_2 bandgap and close to the CB minimum may be created due to the presence of oxygen vacancies (V_Os), Ti^{3+}, and 3d metal dopants (M); purple states close to the VB maximum may be created upon doping with nonmetal impurities (e.g., N, S, C). The relative energetic positions of water splitting redox potentials at pH = 0 (red dashed lines) and CO_2 reduction products (orange dashed lines) are displayed versus the reversible hydrogen electrode (RHE) and the vacuum level.

Historically, the limited light absorption has been tackled, instead, by doping TiO_2 nanomaterials with foreign atoms. Doping of TiO_2 nanomaterials produces colored TiO_2, which are materials with modified electronic structure due to the introduction of suitable "intra-bandgap" electronic states that modify TiO_2 light absorption and optical properties.

Early work on doped TiO_2 employed transition metals (e.g., V, Cr, Mn, Fe, and Cu) introduced as substitutional atoms inside the crystalline habit to generate 3d electronic states lying in the range 0.5−1.5 eV below the CB of TiO_2 and thus providing visible light absorption and photocatalytic efficiency (Figure 1). However, metal doping showed an unfavorable trade-off between absorption and photocatalytic activity, being often responsible for increased charge recombination via newly formed deep electronic levels.[16]

In contrast, nonmetal (e.g., N, C, and S) doping has shown great potential in forming efficient visible light active TiO_2 photocatalysts, typically due to the formation of 2p electronic states above the VB capable of producing efficient charge transfer electronic transition to the 3d CB of TiO_2 and thus providing high photocatalytic activities (Figure 1).

For example, N-doping was reported to yield yellow TiO_2 powders exhibiting a red shift of the optical absorption onset up to ~500 nm.[17] However, in some cases, N or C species induce only a surface modification[18] of TiO_2 rather than bulk doping.

TiO_2 powders of various other colors have also been reported. Liu et al.[19] developed an alternative version of nitrogen doping to produce red TiO_2 anatase microspheres; the reported methodology relied on predoping TiO_2 with interstitial boron atoms. The predoping process improved the solubility of substitutional N atoms in the lattice of anatase TiO_2 and limited at the same time the formation of Ti^{3+} centers as extra electron from B atoms compensating the charge difference between lattice O^{2-} and substitutional N^{3-}. Red TiO_2 was found to absorb the full visible light spectrum and exhibited an optical E_g that varied from ~1.9 eV on the surface to 3.2 eV in the core, as a consequence of the introduced boron concentration gradient.[19,20] Interestingly, the finding did not generate follow-up work in photocatalysis.

Tian et al.[21] reported the preparation of green TiO_2. The green color originated from a charge-transfer complex involving hydrazine groups linked to surface Ti^{4+} centers; green anatase powders showed a broadband light absorption in the visible region that extended also to the near-infrared (NIR) range (~1100 nm), with an optical band gap of 1.05 eV. These examples are based on doping (or codoping) of TiO_2 with extrinsic donor or acceptor species.

However, colored TiO_2 can also be formed by intrinsic doping, namely by the introduction of oxygen vacancies (V_Os) and formation of Ti^{3+} centers in the TiO_2 lattice.

The synthesis of these materials is usually carried out by a high-temperature treatment of TiO_2 in various reducing atmospheres (e.g., vacuum, Ar, H_2/Ar, and pure H_2).[22−24] TiO_2 can be obtained with a gray, blue, brown, or black color depending on the utilized conditions. The resulting color is ascribed to the formation of various amounts of Ti^{3+} and V_Os. Increasing the "level" of reduction leads, in general, to a higher density of defects (e.g., Ti^{3+} and V_O concentration) and consequently to "darker" TiO_2 powders.

In 2011, Chen et al. reported the first black TiO_2 nanomaterial for photocatalysis.[25] Upon a thermal treatment at 200 °C under high pressure of H_2, stoichiometric anatase TiO_2 was converted in defective nanocrystals with high visible light absorption (Figure 2a) and high photocatalytic activity for H_2 generation during photoreforming of water/methanol mixture if a Pt cocatalyst was used. The enhanced performance of black TiO_2 was related to the increased light absorption due to introduction of lattice disorder and H-doping, which consequently narrowed the optical bandgap of black TiO_2 to 1.54 eV by introducing electronic states forming significant VB

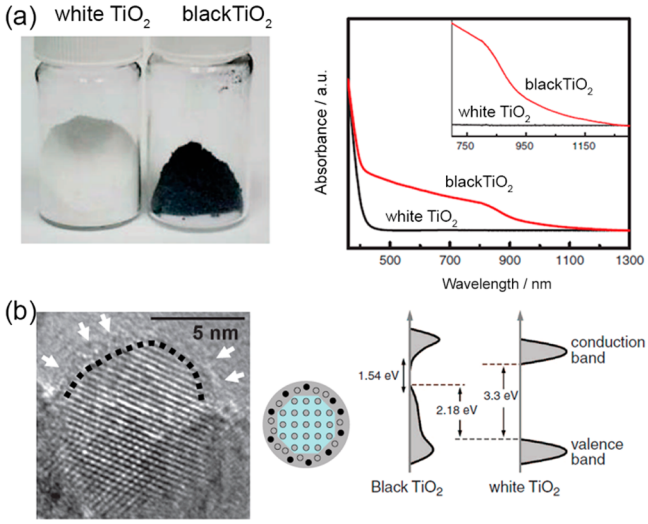

Figure 2. (a) Pictures and absorption spectra of white and black TiO_2 powders synthesized through high-pressure hydrogenation. (b) High-resolution transmission electron micrograph and schematics showing the disordered shell of black TiO_2 and its electronic density of states (DOS). Reproduced with permission from ref 25. Copyright 2011 American Association for the Advancement of Science.

DOI: 10.1021/acscatal.8b04068
ACS Catal. 2019, 9, 345−364

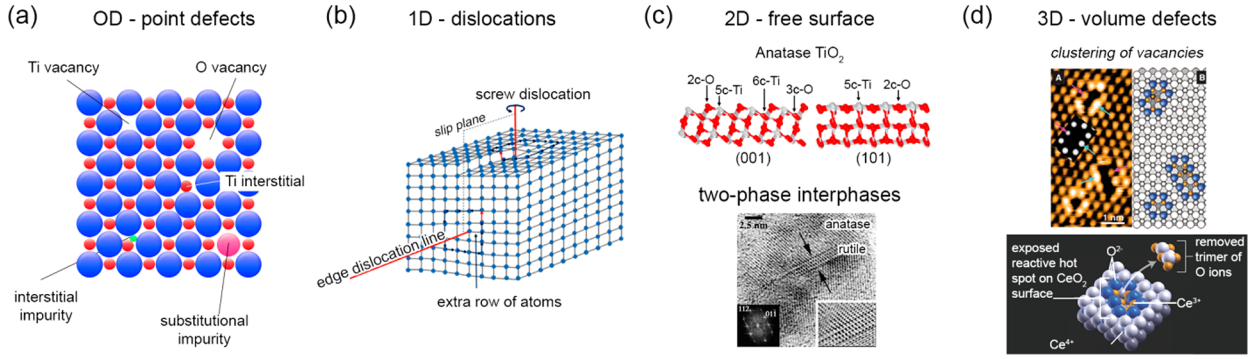

Figure 3. (a) Schematics of possible crystal defects in TiO_2. (b) Generic representation of linear defects (dislocations) in an inorganic nanocrystal. (c) Upper figure: unrelaxed anatase TiO_2 (001) and (101) surface. Lower figure: a rutile inclusion grown inside an anatase crystal. (d) Upper figure: scanning tunneling microscopy (STM) image of triple linear surface oxygen vacancies on CeO_2 (111) surface and corresponding structural model. Lower figure: schematic representation of defect clustering shown in STM of upper figure. (b) Reproduced with permission from ref 54. Copyright 2014 Springer. (c) Upper figure: reproduced with permission from ref 59. Copyright 2008 Nature Publishing Group. Lower figure: reproduced with permission from ref 60. Copyright 1999 mineralogical Society of America. (d) Reproduced with permission from refs 61,62. Copyright 2005 American Association for the Advancement of Science.

and CB tailing (Figure 2b). An interesting feature of this type of core−shell black nanocrystals was the sharp optical absorption band edge shown at ∼1000 nm.

A myriad of material designs, from H-doping to defect engineering, have appeared since 2011 and have produced reduced TiO_2 nanomaterials with enhanced (or not) photocatalytic performance and having various colors from green, yellow, blue, and back to black,[26−28] as well as an important "gray" version.[29,30]

Despite early studies on reduced TiO_2 that started in the 50s[31−33] and significantly progressed with the advent of scanning tunneling microscopy (STM) and surface science,[34] the renewed interest in the past decade on defective oxides for photocatalysis has enabled the discovery of new materials and phenomena, holding great promise to further boost the advances toward solar fuel generation.

Recently, the synthesis of gray TiO_2 nanomaterials showing high photocatalytic H_2 production by operating under cocatalyst-free conditions has been reported, opening new opportunities in the design of catalytic sites for photocatalysis.[29,35−37]

In particular, Liu et al. introduced several preparation methods to reduce TiO_2 nanopowders[29,30,38] and nanotubes[35,39] to form partially reduced materials with stable and very high photocatalytic hydrogen production without the use of any noble metal cocatalyst. The high-temperature, high-pressure (500 °C, 20 bar) hydrogenation of anatase or mixed anatase/rutile TiO_2 produced unique catalytic sites that enabled cocatalyst-free hydrogen production rate that were 2 orders of magnitude higher than those observed for stoichiometric powders, reaching values of more than 200 μmol g^{-1} h^{-1}. Later on, other synthetic procedures, such as high energy ion implantation,[39] hydride ball milling,[38] and partial oxidation of TiN powders,[40] have been shown to produce similar reduced TiO_2 varieties producing hydrogen without any addition of noble metals.

The use of various forms and structures of hydrogenated TiO_2, black TiO_2, or more generally reduced TiO_2 have meanwhile also shown superior activity when used as photoanodes for photoelectrochemical water splitting.[41−49] Recent findings have unveiled that a major contribution to the working mechanism of reduced titania electrodes is given by the enhanced conductivity,[50] while others argue a higher donor density of black TiO_2, resulting in higher band bending and therefore charge separation at the electrode/electrolyte interface.[51] Further studies are needed and might reveal specific roles of defects in addressing photoelectrochemical selectivity during water splitting (i.e., two-electron vs four-electron oxidation). These aspects have been recently reviewed and thus they will not be covered in this Review.[52]

Nevertheless, the common line that underlies black TiO_2 research is the mismatch among the amount of increased absorption or band gap narrowing and the corresponding photocatalytic activity; although light in the visible range may be absorbed, no visible light reaction activity may be observed.

Relevant questions that emerge from a literature survey are the following: (i) Where are visible photons lost during the photocatalytic process? (ii) What is the best material design to increase both absorption and photocatalytic activity? (iii) What is the subtle connection among crystal defects, structural and electronic singularities, light absorption, charge separation, and photocatalysis?

In this Review, we provide some answers to these questions with the aid of current knowledge and give a brief overview on defective TiO_2 nanomaterials for photocatalysis, drawing relationships that interlink structural and electronic features in TiO_2 to photoconversion efficiency.

In particular, we will cover the type of crystal defects in TiO_2 and the consequences that they bring on lattice geometry as well as on electronic DOS. We present electron paramagnetic resonance spectroscopy (EPR) as a useful technique that provides plenty of information both on crystal structure and extra electrons hosted in TiO_2 due to creation of crystal defects.

With this in mind, we will discuss several surface science studies on TiO_2 photocatalysis that are, in our opinion, fundamental to tackle a rational design of defective black TiO_2 for photocatalysis.

We will describe the different types of defects formed in various black TiO_2 nanocrystals and review how they influence the photocatalytic hydrogen production by using water splitting or photoreforming of alcohols. This last section is dedicated to photocatalysis with black TiO_2 and covers with a critical view the development of photocatalysts from core−shell nanocrystals and phase nanojunctions to cocatalyst-free black TiO_2.

DOI: 10.1021/acscatal.8b04068
ACS Catal. 2019, 9, 345−364

2. DEFECTS IN METAL OXIDES: THE CASE OF TiO_2

2.1. Types of Crystal Defects and Relation with Photocatalysis. A large variety of physical properties of crystalline material is regulated by the presence of different types of defects and imperfections. Defects engineering indeed plays a prominent role in tailoring electronic, magnetic, optical, mechanical, and quantum properties as well as it is crucial for activation of heterogeneous (photo)catalytic processes.[53]

The classification of crystal defects is generally made according to the dimensionality of the defect.[54,55] Zero-dimensional (0D) defects are related to a single or a few atomic positions and hence are called *point defects* (Figure 3a). In any TiO_2 nanocrystal, we may find therefore several point defects such as Ti vacancy Ti_V (rare), Ti interstitial Ti_i (common and important for photocatalysis), O vacancy V_O (often observed in reduced TiO_2), and interstitial (e.g., hydrogen or nonmetal dopants) or substitutional impurity (e.g., metal or nonmetal dopants).

The introduction of point defects produces structural rearrangements that may create significant distortions in the local symmetry of Ti octahedra, thus influencing the charge transport and recombination during photocatalysis. This topic will be discussed in more detail in Section 2.2.

Similarly, the direct consequence of the introduction of 0D defects on electronic DOS of TiO_2 depends on their specific nature, and several excellent reviews provide in depth discussion on this aspect.[10,15]

Substitutional metal dopants generally contribute to DOS through additional 3d states forming below the CB of TiO_2 (Figure 1). A similar electronic effect is found when a significant amount of V_Os is generated, with the mutual formation of Ti^{3+} charged sites producing electronic states 0.8−1.2 eV below the CB.[56] Otherwise, nonmetal dopants (e.g., N, C, S) and interstitials (e.g., H or Ti) present electronic features that populate the DOS of defective TiO_2 in the region above the VB, providing a more effective strategy than metal doping to modify TiO_2 electronic structure (Figure 1 and 2b).[25,26,56,57] Electronic transitions from 2p states due to nonmetal dopants to CB are usually very efficient and produce a positive trade-off between optical absorption and photocatalytic efficiency. Otherwise, metal centers producing excess of electronic states below the CB, once exceeding a specific threshold, behave like recombination centers for photogenerated charges, thus being detrimental for photocatalytic reactions.[58]

The physical location of point defects is another important feature, which has great influence in the electronic DOS of TiO_2 and its photoreactivity. Point defects can be positioned at three different locations: (i) at the surface, defined as the first atomic layer of a nanocrystal; (ii) at the subsurface, defined as the crystal slab contained between the second layer from the surface and including few nanometers in depth; and (ii) in the bulk of the nanocrystal.

Linear or 1D defects are generally called *dislocations* and produce lattice strain (Figure 3b), which has been reported to be beneficial for photocatalytic activity with TiO_2. Dislocations are the result of plastic deformation of crystal lattice and identify the area where the crystallographic registry is lost.[55] The 2D defects that appear in crystals can be usefully classified into three groups: *free surfaces* exposing uncoordinated atoms (see Figure 3c), interphases within a crystal such as *stacking faults* and *antiphase boundaries*, and other various types of boundaries, for instance, grain boundaries and two-phase boundaries (interphases). For TiO_2 photocatalysts, 2D defects are especially important and dictate surface reactivity as well as charge transport and separation in the bulk, for example by creating anatase/rutile nanojunctions (Figure 3c).[60]

Volume defects (3D) mainly cover inclusions, crack, voids, and pores. Here, we consider more relevant to our purpose the discussion on voids created by the clustering of V_Os and their effects on reactivity of TiO_2. Many reports have shown that clustering of vacancies is a prominent phenomenon observed in a wide range of metal oxides ranging from CeO_2[61,62] and simple perovskites (i.e., $SrTiO_3$)[63,64] to double perovskites, where it is responsible for a large change in magnetoresistance response.[65,66] A relevant case is CeO_2 that is considered a prototypical reducible oxide due to its high *"oxygen storage capacity"*. This property makes CeO_2 a fundamental component of modern automotive exhaust treatment, with V_Os and their linear clustering, determining reactivity of CeO_2 catalysts (Figure 3d).[61,62] Ensembles of V_Os have been also observed at the interface of $SrTiO_3$ and $LaAlO_3$ thin films, being responsible for the formation of electron gas at the interface between these two perovskites.[67] Although there is no clear evidence so far for the formation of such 3D defects in reduced TiO_2, all these examples suggest that they may play prominent role in the physics and chemical reactivity of TiO_2.

Finally, an interesting case study is the situation when more than one type of defects forms at the same time. This particular *"defects pairing"* is often overlooked in photocatalysis, mostly due to the challenge behind its structural and electronic characterization. A seminal contribution from Diebold et al. provided evidence for such *defect pairing* through STM images and density functional theory (DFT) calculations.[68] A reduced anatase (101) crystal showed ordered subsurface V_Os in STM, consistent with DFT results predicting that V_Os at subsurface and in bulk have a lower formation energy than those on the surface; here it is noteworthy that defects on rutile remain on the surface.[68] Therefore, defective polymorphs may behave entirely differently in photocatalysis. The formation of ordered subsurface defects invokes a Frenkel hop mechanism (Figure 4). It relies on the formation of V_Os that induces the migration of a neighboring Ti atom to an interstitial site (T_i), leaving behind a Ti_V. This process is repeated producing a series of Ti_i-Ti_V pairs.[68] In photocatalysis with reduced TiO_2, V_Os are usually considered, but *defect pairing* should be also taken into account, and more efforts should be put to elucidate the connection between different types of defects to shine light on important aspects of photocatalytic processes.

2.2. Defects in Reduced TiO_2: An Atomistic View from Electron Paramagnetic Resonance (EPR) Spectroscopy. Continuous wave (CW) X-band EPR spectroscopy has been used extensively to address nature and stability of the spin centers present in the TiO_2 photocatalyst, before, during, and after light irradiation experiments. The most common paramagnetic centers encountered in various TiO_2 preparations, from nanoparticles to nanotubes, are those associated with the presence of Ti^{3+} sites ($3d^1$, $S = 1/2$) from the diamagnetic Ti^{4+} sites and oxygen-based radicals ($S = 1/2$, $-O^{-\bullet}$, $-O_2^{\bullet-}$). These "spin-active defects" can be embedded in the lattice or formed on the material's surface. The most studied polymorphs of TiO_2 for the water splitting processes are anatase and rutile. Both systems have tetragonal crystal structures. However, anatase shows space group $I4_1/amd$ (unit cell, $a = 3.7845$, $c = 9.5143$ Å), while rutile expresses the space

DOI: 10.1021/acscatal.8b04068
ACS Catal. 2019, 9, 345−364

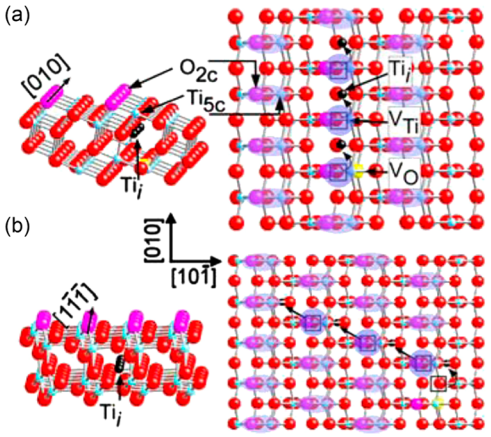

Figure 4. (a), (b) Models of anatase TiO_2 (101) in side (left) and top (right) view (red balls: O; light blue balls: T_i) illustrating the formation of clustering of subsurface defects along open channels parallel to the crystallographic (a) [010] and (b) [111] directions. Formation of a subsurface O vacancy (V_O) (yellow) initiates the migration of a neighboring Ti atom to an interstitial site (Ti_i, black), leaving behind a Ti vacancy (V_{Ti}, black square). Reproduced from ref 68. Copyright 2009 American Physical Society.

group $P4_2/mnm$ (unit cell a = 4.5937, c = 2.9587 Å). The magnetic moments arising from formation of the spin-containing centers, Ti^{3+} and oxygen-based radicals, are very sensitive probes that screen even minor alterations of their surroundings (ligand-field). The contribution of orbital angular momentum to the spin angular momentum shifts their g_{eff} values away from the free electron value, g_e = 2.0023. The extent of the shift from g_e is proportional to the spin−orbit coupling constant, and anisotropic resonances ($g_{x,y,z}$) arise from distortions in the crystal-field symmetries, which lift the frontier orbitals degeneracies. Therefore, in TiO_2 materials the g_{eff} values observed for the spin-defects can be grouped into two categories; (i) spin-containing centers that feature larger g-values than the free-electron in the vacuum and (ii) those with smaller g-values. This implies that from EPR measurements a rich set of information regarding both the structural deformation and the electronic features introduced by formation of defects is obtained. Formation of Ti^{3+} sites in TiO_2 gives g_{eff} < 2.0023, with resonance signals that are most often described in term of S = 1/2 center embedded in a tetragonal-field (D_{4h}). The g-value observed for oxygen-based radical in TiO_2 falls at g_{eff} > 2.0023, and the observed g-tensor components are consistent with axial or rhombic S = 1/2 systems. Figure 5 collects a series of simulated CW X-band EPR spectra obtained in the spin-Hamiltonian framework by perturbation theory (SimFonia software V.1.25) showing the most common fingerprints expressed by defective centers in TiO_2.

The g-tensor values used in the simulated spectra have been taken from literature data. Figure 5a illustrates the EPR envelope of Ti^{3+} sites in regular lattice position found for anatase single crystal,[69] and Figure 5b the EPR resonance for trapped electrons in the rutile phase (Ti^{3+} in regular sites).[70] EPR study of interstitial Ti^{3+} centers have been analyzed using single crystal rutile phase by Aono and co-workers (termed A-spectrum)[71] and have been observed earlier by Chester (termed C-spectrum).[70] The authors[69] showed that when exchange interactions are negligible, that is, when the interstitial Ti^{3+} centers are separated far away from each other ($d \gg$ 3.25 Å), the g-tensor components observed are similar to those seen for Ti^{3+} sites located in the regular lattice position (see Figure 5b, right panels for details). When two Ti^{3+} sites become close to each other in space ($d \leq$ 3.25 Å), effective exchange coupling occurs and the emerging S = 1 spin-state produces triplet-signals (termed X-spectrum) with g_x = 1.9846, g_y = 1.9802, and g_z = 1.9509.[72]

Recently, Chiesa and coauthors reported the observation of another type of high-spin EPR signal, best seen at Q-band frequency, which was obtained during the controlled oxidation of a Ti precursor in the synthesis of TiO_2 (anatase). They observed formation of an isotropic signal (g_{iso} = 1.973) that pointed toward formation of four magnetically coupled Ti^{3+} centers (S = 2) showing small zero-field-splitting parameters (zsf), with estimated |D|= 76 MHz and |E|= 4 MHz), thus large interspin-distances, in the range of 5−10 Å.[73]

Larger zero-field-splitting (zfs) spin-triplets associated with Ti^{3+} sites residing in the regular lattice position have also been reported to form upon photoexcitation in rutile crystals (λ = 442 nm).[74] Here, neutral V_Os were generated, with two trapped electrons that were localized on two of the three cations adjacent to the V_O, forming a pair of exchange-coupled Ti^{3+} ions with a ground state formed by close lying singlet (S = 0) and triplet (S = 1) states. Figure 5f shows a rendering of the literature data from Brant and co-workers in which two equally intense and widely separated lines (~538 G) have been recorded along the [001] direction, and visible at cryogenic temperatures (T = 25 K, with g-tensor, g_1 = 1.9582, g_2 = 1.9138, g_3 = 1.8262).[74]

In contrast, Figure 5c shows the broad EPR resonance signal characteristic of surface exposed Ti^{3+} sites, where an isotropic resonance line is mainly expected, due to the surface disorder.[75] In particular, this type of signal appears to be very sensitive to the specific TiO_2 synthesis employed, especially when heavily reduced TiO_2 materials are aimed. For example, in some "pale gray-blue" anatase, the signal addressable to the surface exposed Ti^{3+} becomes not only very broad but also characterized by an anisotropic g-tensor (g_x= 1.9452, g_y = 1.918, and g_z = 1.875), hence having g_{eff} as small as 1.913.[76]

Figure 5d shows the sharp signal featuring isotropic g-value close to the free electron in the vacuum that has been analyzed in the literature as electrons trapped in V_O (called in literature F or F^+ center).[77−79] However, it should be mentioned that excess electrons are preferentially trapped by the Ti^{4+} ions in TiO_2-based materials, and therefore, the physical origin of such signal remains in the literature as a matter of controversy. Sun and coauthors[77] reported the preparation of titania nanoparticles by hot wall low pressure MOCVD method in which the resonance attributed from F-centers was observed even at high temperature (T = 473 K). Although the EPR intensity $I(T,t)$ changed with temperature T and time t, the g factor of such signal remained constant, at 2.0034. A similar signal was reported earlier by Nakamura and coauthors (F, F^+ centers) from plasma-treated TiO_2 powders, which was characterized by comparable g_{iso} value (g_{iso} = 2.004 at T = 77 K).[78] Other groups have addressed such defects in terms of medium polarized electrons ubiquitously present in reduced TiO_2 and have been associated with the CB or have been described as defect state at the particle−particle interfaces.[80] In the latter case, the EPR resonance displayed nearly identical isotropic envelopes, similar to Sun and Nakamura's works, but were characterized by lower g-values, falling in between 2.0011−

DOI: 10.1021/acscatal.8b04068
ACS Catal. 2019, 9, 345−364

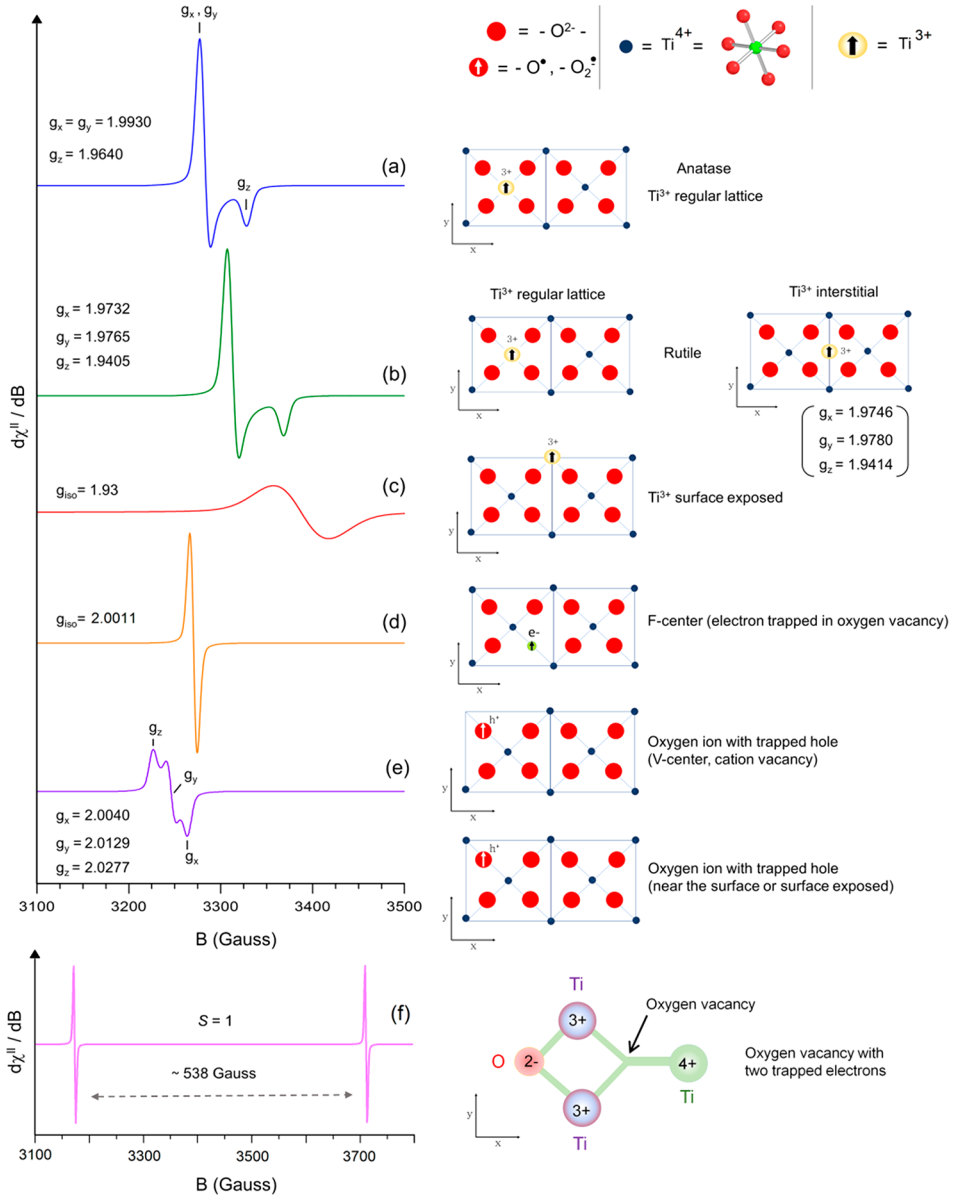

Figure 5. Simulation of X-band EPR spectra arising from the spin containing centers usually formed in TiO_2 materials from synthesis. The spectra (a) to (c) are associated with Ti^{3+} sites (S = 1/2), spectrum (e) is associated with oxygen-based radical (S = 1/2, $-O^{\bullet-}$ radical), and (d) to defects, termed F-centers, that are either directly associated with Ti^{3+} sites or to the oxygen-based radical sites. Spectrum (f) shows a rendering of the signature obtained on the single crystal rutile along the [001] direction, due to exchange coupled Ti^{3+}–Ti^{3+} centers (S = 1). The simulations were obtained by perturbation theory, using g-values (a–e) that are given along the EPR traces. The frequency used to generate the spectra was 9.1500 GHz, the line-width tensor used ($LW_{x,y,z}$ in Gauss) were 10,10,10 in (a), (b); 60,60,60 in (c); 8,8,8 in (d) and (e), 4,4,4 in (f). All the spectra were obtained using a Lorentzian/Gaussian ratio of 0.63 and spherical integration with theta, phi of 200, 200. The drawings shown on the right illustrate the probable positions in the lattice of the spin containing defects, by looking at the crystal packing along the x,y plane.

2.0025. A note of caution should thus be given when such sharp EPR signal is observed, because it can arise from carbon centered impurities being adventitiously present in many TiO_2 materials. For example, Minnekhavov and coauthors demonstrated that similar EPR signals and g-values as those attributed to arise from F/F^+ centers emerge clearly in carbon-doped TiO_2 materials and these types of resonances and g-values are associated with electrons being trapped on the carbon-sites (C content of 0.46–1.05% w, g_{iso} values of 2.0030 ± 0.0005).[81] Spin centers associated with positive holes (h^+) are formed in TiO_2 upon light exposure/irradiation and are known to be located on oxygen sites, directly on the surface, although they can also be formed in the subsurface regions.[82−84]

Figure 5e shows the simulated EPR spectrum for the $-O^{\bullet-}$ radical ion observed in a rutile single crystal.[85] Similar g-tensor parameters have also been observed for the $-O^{\bullet-}$ radical sites in synthetic anatase single crystals (g_x = 2.0029, g_y = 2.0140, and g_z = 2.0265) by Grunin and coauthors.[86] Other oxygen-based radical centers, such as superoxide radical anions ($O_2^{\bullet-}$) obtained under UV–vis irradiation, express similar spin-Hamiltonian parameters and resonance envelopes likewise $-O^{\bullet-}$, with g_x = 2.0026–20019, g_y = 2.011–2.0014, and g_z = 2.007–2.001, in both anatase and mixed (anatase/rutile) phases.[87−89] Larger g-anisotropy is found for surface-exposed Ti^{4+}-$O_2H^{\bullet}$ radicals, photogenerated from TiO_2 material containing preadsorbed oxygen (g_1 = 2.034, g_2 = 2.008–

DOI: 10.1021/acscatal.8b04068
ACS Catal. 2019, 9, 345−364

2.009, and g_3= 2.002). These species usually exhibit broader EPR signals compared to -$O^{\bullet-}$ radicals.[90,91]

Figure 6 shows the X-band EPR spectra (T = 80 K) obtained for anatase powder as delivered (commercial anatase powder,

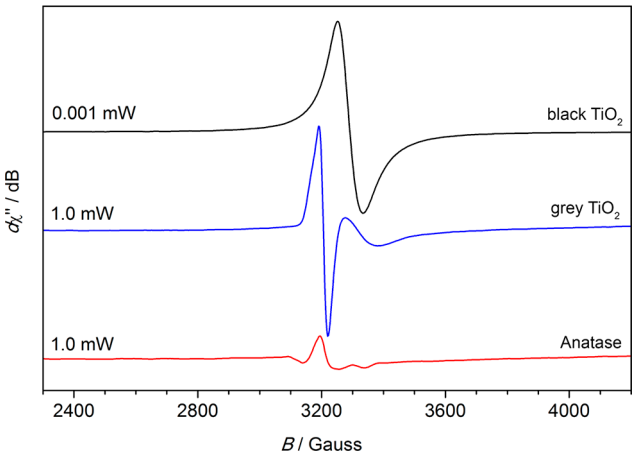

Figure 6. X-band (8.960 GHz, T = 80 K) EPR spectra of commercial anatase powder (red trace), gray anatase (reduced at 500 °C, H500, blue trace) and black anatase (reduced at 700 °C in H_2, H700, black trace). Experimental parameters: modulation frequency 100 kHz, modulation width of 2.0 mT and time constant 0.1 s. The different microwave powers employed during signal acquisition are reported next to each resonance signal for easier comparison. Adapted from ref 29. Copyright 2016 Wiley-VCH.

25 nm, 99.7% purity) and upon thermal hydrogenation at temperatures of 500 °C, coded as H500 (gray anatase) and 700 °C, coded as H700 (black anatase), as recently reported by Liu and coauthors.[29] The pristine anatase sample (Figure 6, red trace) shows only a weak paramagnetic signal, arising from the presence of both Ti^{3+} sites ($g_{eff}<g_e$) and h^+ holes ($g_{eff} > g_e$). The gray anatase sample (H500) and the black anatase (H700) show drastic changes in the resonance envelope. The gray anatase (H500) gives a strong paramagnetic signature that has been interpreted by the authors with the response of two species (g_x = 1.90, g_y = 1.92, g_z = 1.985 for one species and g_x = 1.998, g_y = 1.998, g_z = 1.99 for the other). The black anatase sample (H700) shows the appearance of a very strong signal, well in line with other reports on "black" TiO_2.[25,56,92,93] The EPR signature of H700 gives g-tensor values of g_x = 1.975, g_y = 1.940, g_z = 1.895, and these paramagnetic signals were attributed by the authors to formation of Ti^{3+}/V_O centers introduced into the TiO_2 lattice by the thermal reductive treatment.

Therefore, the number and signature of spin active Ti^{3+} sites compared to commercial anatase is one of the contributing factors underneath the different catalytic performance of "black" TiO_2 and gray anatase. While gray anatase shows significant photocatalytic H_2 activity, black TiO_2 does not if no Pt cocatalyst is applied.[29] The example illustrates that the simple increase of the number of spin containing defects should not be considered as the universal synthetic strategy to pursue in the material design, namely the only way to improve catalysis. Clearly the gray (H500) material contains less paramagnetic species than the black material, but is active for an H_2 evolution process (75 μmol h^{-1} g^{-1}). In other words, concentration and nature of defects play a role in designing desired effects. As recently discussed by several groups,[58,94,95] the introduction of V_Os does, on one hand, improve the UV and visible-light photocatalytic activity but leads as well to trapping of electrons below the CB, an effect that does reduce the lifetime of photogenerated charge carriers, and points toward a reduction in the catalytic performance.

3. SURFACE REACTIVITY IN REDUCED TiO_2 SINGLE CRYSTALS

In this section, we discuss significant investigations performed with ultrahigh vacuum techniques that, combining atomically resolved STM to electronic spectroscopies, have provided key advancements in the understanding of (photo)reactivity in reduced TiO_2 single crystal surfaces. More details can be found in excellent reviews dedicated to the subject.[96−98]

The results from surface science studies are often overlooked in photocatalysis with black (and partly reduced) TiO_2, although these ideal examples have demonstrated fundamental properties of reduced TiO_2 that may be still valid under operational conditions, thus providing important guidelines for understanding structure−activity relationships in black TiO_2.

For instance, a crucial structural feature of TiO_2 is the formation of surface V_O upon thermal reduction. The most general mis-assignment in black TiO_2 research is the presence of surface V_Os in anatase TiO_2. Many groups have reported indeed STM proofs and DFT calculations showing that surface V_Os are stabilized only in rutile TiO_2, while for anatase V_Os have too low rearrangement energy to migrate toward subsurface layers (Figure 7a,b).[68,99−101] The difference in topology of the defective site in anatase and rutile is responsible for the different nature of electronic states. In particular, two O atoms surround the anatase V_O, both bonded to two Ti neighbors; whereas in rutile, three O atoms surround the V_O, with two of them having same symmetry as for anatase, while the third O is bonded only to one Ti (Figure 7c). As a consequence, V_Os in rutile induce only deep localized electronic levels. In anatase, instead, V_Os can induce shallow electronic levels, high in energy and strongly delocalized, together with deep and localized levels.[101] These aspects have been also experimentally pointed out by EPR measurements by comparing the ^{17}O hyperfine coupling typical of oxygen ions surrounding paramagnetic Ti^{3+} centers in anatase and rutile[75,102] with those of a well-defined molecular system where electron density is confined in the limits of the molecule.[103] These shallow electronic levels in anatase may account for the superior electron transport in anatase,[104,105] electron diffusion to the surface as well as a reduced electron−hole recombination.

These properties crucially improve the photocatalytic activity of reduced anatase TiO_2, which is often reported to be orders of magnitude higher than reduced rutile.

Figure 8a shows the reduced rutile r−TiO_2 (110) surface (i.e., the most studied in STM), which consists of alternating rows of 5-fold-coordinated Ti_{5c} atoms (bright rows) and 2-fold-coordinated O_{br} atoms (dark troughs).[98] The faint protrusions observed between T_{5c} and O_{br} rows represent V_Os (see square in Figure 8a) formed upon ion bombardment. Upon hydration, H_2O molecules dissociate in V_O sites and the resulting STM image (Figure 8b, h−TiO_2) shows the consequent formation of OH groups.[106] In contrast, H_2O molecules have been observed to form local ordered superstructures due to charge rearrangement at anatase surface.[107] Otherwise, the interaction of O_2 with rutile r−TiO_2 (110) surface produces the healing of V_Os and the

DOI: 10.1021/acscatal.8b04068
ACS Catal. 2019, 9, 345−364

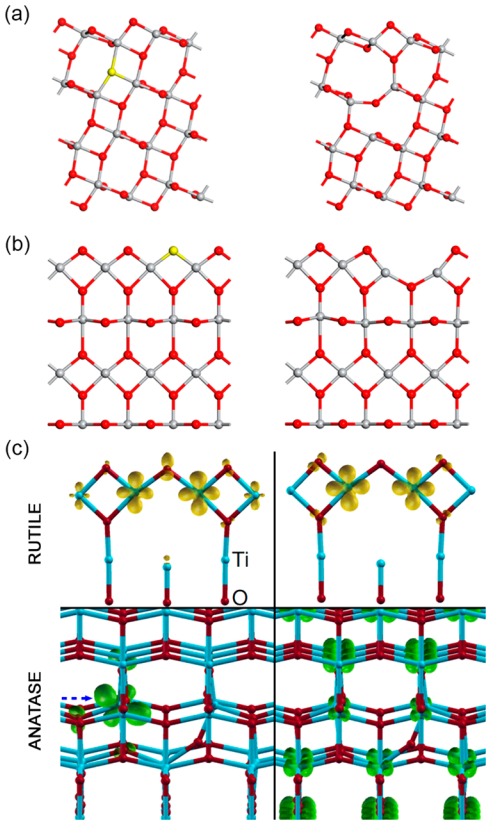

Figure 7. Atomic slab models of (a) anatase (101) and (b) rutile (110) surface. The slabs on the left represent perfect crystals without defects, and the slabs on the right are the surface structure with an oxygen vacancy after geometry relaxation. (c) Spin density distributions of defect states induced by an oxygen vacancy for both rutile and anatase. (a,b) Reproduced from ref 99. Copyright 2015 American Chemical Society. (c) Reproduced from ref 101. Copyright 2008 American Physical Society.

formation of O adatoms located on the top of T_{5c} (Figure 8b, see circle and ellipse). Starting from *h*−TiO_2 (Figure 8c) and exposing it to increasing amount of O_2, a characteristic electronic signature was discovered. The VB spectra were also retrieved accordingly from photoelectron spectroscopy (PES) experiments.[106] The pristine *h*−TiO_2 (Figure 8g) showed additional electronic states due to (i) OH 3σ at ∼10.8 eV and (ii) Ti 3d at 0.85 eV below the Fermi level. Increasing amount of O_2 completely quenched the OH electronic states much faster that those related to Ti 3d (Figure 8c−f STM images; g and h PES spectra and PES normalized area corresponding to OH and Ti 3d states). Interestingly, at 4 Langmuirs (L) of O_2 exposure the rutile surface (Figure 8d) was completely recovered from OH (or H capping atoms) and V_Os, while it was still showing elongated bright spots and significant Ti 3d states. Subsequently, experiments carried out at different temperature under O_2 exposure revealed the nature of this protrusion and of electronic states below Fermi level. This set of experiments is particularly important since it provided strong evidence that the nature of intragap electronic states above VB was due neither to V_Os nor to H capping atoms (OH groups), but was related to the formation of interstitial Ti atoms (T_i) present on the subsurface.[106] Importantly, other reports have also shown that subsurface Ti_i, either in rutile or anatase single crystals, may stabilize molecular adsorbate such as H_2O, O_2, methanol, and ethanol through charge transfer

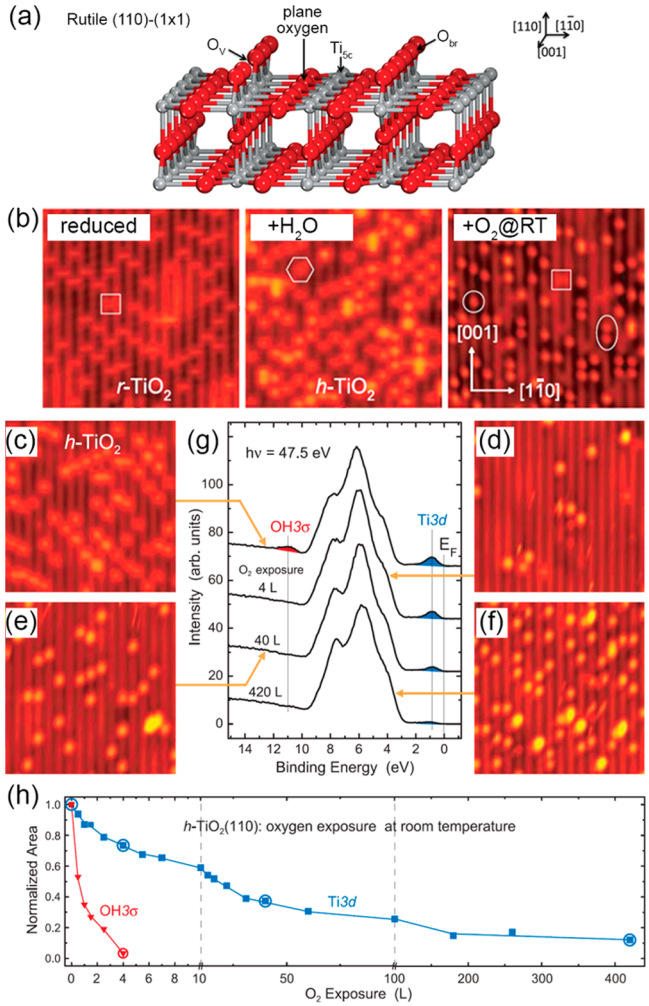

Figure 8. (a) Structure model of rutile (110)-(1 × 1) (*r*-TiO_2(110)-(1 × 1)). Red and gray balls stand for O and Ti ions, respectively. (b) STM images (105 by 105 Å) recorded at temperatures between 100 and 130 K of reduced *r*-TiO_2(110), hydrated *h*-TiO_2(110), and a room temperature (RT) O_2-saturated TiO_2(110) reduced surface. Symbols indicate O_{br} vacancies (square), capping H atoms (hexagon) in the O_{br} rows, and O_{ot} adatoms (circle), as well as pairs of next-nearest O_{ot} adatoms (ellipse) in the Ti troughs. (c−f) STM images (105 by 105 Å) of a reduced *h*-TiO_2(110) surface that was exposed to increasing amounts of O_2 at RT. (g) Selected VB-PES spectra recorded on a reduced *h*-TiO_2(110) surface that was exposed to O_2 at RT. Arrows indicate the representative STM images. (h) Normalized integrated intensities of the OH_{3s} (red) and Ti_{3d} (blue) features for O_2 exposures up to 420 L from PES spectra; circles indicate intensity values that were obtained from the spectra shown in (g). (a) Reproduced with permission from ref 98. Copyright 2016 The Royal Society of Chemistry. (b−h) Reproduced with permission from ref 106. Copyright 2008 American Association for the Advancement of Science.

interactions, thus providing an additional pathway for their activation/dissociation both under dark and illumination conditions.[98,108−115]

4. PHOTOCATALYTIC HYDROGEN PRODUCTION WITH REDUCED COLORED TiO_2

4.1. Pt-Modified Black TiO_2. Tremendous interest in black, or more generally colored, TiO_2 has been attracted by the pioneering work of Chen et al.,[25] who used mesoporous

DOI: 10.1021/acscatal.8b04068
ACS Catal. 2019, 9, 345−364

anatase TiO_2 nanocrystals that were exposed to a treatment at 200 °C in pure H_2 at high pressure (20 bar). Such powders, when kept under these conditions for 5 days, turned black, and, when decorated with Pt nanoparticles (NPs), showed a remarkably high (and stable) photocatalytic H_2 generation activity (Figure 9a). A H_2 production rate of 10 mmol h^{-1} g_{cat}^{-1} was observed under solar illumination, while untreated (white) Pt-TiO_2 powders resulted inactive. Similar results were observed in methylene blue photocatalytic oxidation tests (Figure 9b). Upon hydrogenation, crystallographic disorder was introduced at the surface of TiO_2 nanocrystals, forming crystalline−amorphous core−shell black TiO_2 with intense light absorption in the visible and NIR spectral range, originating from the narrowing of TiO_2 bandgap from 3.30 to 1.54 eV (see Figure 2).

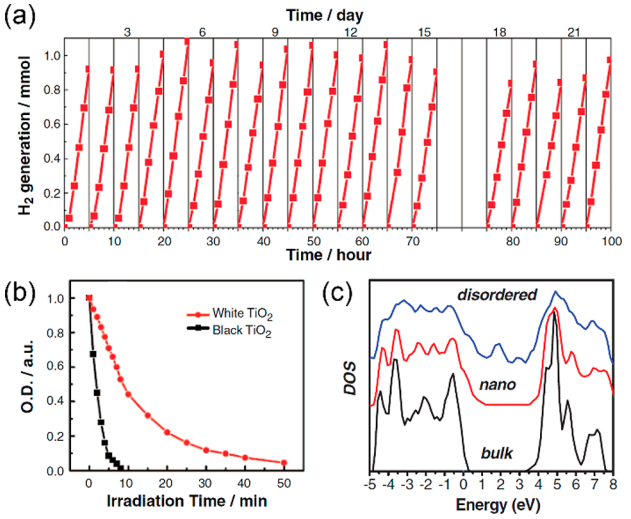

Figure 9. (a) Cycling measurements of H_2 generation through direct photocatalytic water splitting with disorder-engineered black TiO_2 nanocrystals under simulated solar light; (b) Comparison of the solar-driven photocatalytic activity of black TiO_2 nanocrystals with that of white TiO_2 nanocrystals under the same experimental conditions (y axis: optical density of the methylene blue solution); (c) Calculated density of states (DOS) of black TiO_2 in the form of a disorder-engineered nanocrystal, a stoichiometric nanocrystal (nano), and a bulk crystal. The energy of the valence band maximum of the bulk phase was taken to be zero. Reproduced from ref 25. Copyright 2011 American Association for the Advancement of Science.

The stark variation of the optical properties was assigned, by VB XPS analysis and first-principle DFT calculations, to a "tailing" (broadening) of VB and CB (Figure 9c), ascribed to the formation of a disorder shell containing Ti−H and −OH bonds resulting from the high-pressure treatment.[25,116,117] The authors ascribed the high photocatalytic activity of black powders to the enhanced charge separation of electrons and holes. The former localize into the disordered shell, and close to the surface to reduce H^+ to H_2, while the latter are formed in the crystalline core.[116] Therefore, the absorption of visible and NIR photons may induce transitions between midgap states and the CB tail, which correspond to charge transfer from the O 2p to Ti 3d orbitals (similarly to the efficient transitions leveraged in nonmetal doped TiO_2). Such separation of photoexcited electrons and holes prevents fast recombination, and the visible-NIR light absorption led thus to charge carriers that can efficiently contribute to the photocatalytic process.

However, in this work, high-pressure hydrogenated black TiO_2 powders exhibited a relatively poor H_2 evolution activity of ∼0.1 mmol h^{-1} g_{cat}^{-1} under, visible/NIR illumination (λ > 400 nm), which was 2 orders of magnitude lower than that measured under solar irradiation (10 mmol h^{-1} g_{cat}^{-1}).[25] In spite of the poor visible light performance, these findings triggered a considerable amount of follow-up work, and various reduction strategies and hydrogenation approaches to produce more active black TiO_2 materials have meanwhile been explored.[118−122]

Zheng et al.[118] hydrogenated protonated TiO_2 (H-TiO_2) nanotubes (NTs) into dark brown single crystalline rutile TiO_2 nanowires with a diameter of 8 nm. The treatment was carried out at 500 °C in a H_2/N_2 atmosphere. Such dark brown TiO_2 nanowires were also reported to exhibit strong visible light absorption and, upon Pt decoration, showed a more than three times higher H_2 evolution rate (2.15 mmol h^{-1} g_{cat}^{-1}) compared to untreated structures. The authors claim that such black nanowires can preserve their one-dimensional morphology due to the ability of protonated TiO_2 nanotubes (precursor) to "store" molecular hydrogen: it is suggested that ion exchangeable −OH groups in the titanate lattice can stabilize H_2 molecules via weak van der Waals interactions. Upon annealing, dehydration of nanotubes (removal of crystallographic water) takes place, which leaves behind surface dangling terminations that, from intercalated H_2 molecules, form Ti−H bonds. In other words, the authors proposed that the nanotube surface is by this approach reactive to adsorbed H_2 under relatively mild conditions, and the formation of Ti−H terminations is crucial to stabilize the surface disorder induced by hydrogenation, so that the nanowires can preserve their one-dimensional (1D) morphology.[118] It should be however pointed out that the stability (at room temperature) of such Ti−H terminations was not discussed, and that the authors based their interpretation only on minor differences in the IR and XPS spectra of air- and H_2-treated structures.

Common preparation "protocols" for black TiO_2 photocatalysts mostly involve a preliminary hydrogenation step to blacken TiO_2, which is then surface loaded with Pt nanoparticles by various methods (common metal nanoparticle deposition methods are deposition precipitation, impregnation, photoreduction, and chemical reduction, e.g., with H_2 or $NaBH_4$).[123−125]

Zhu et al.[119] revisited such hydrogenation−Pt decoration sequence, and developed an original approach to introduce surface disorder in TiO_2 powders based on a "H_2 spillover mechanism". For this, Pt NPs were first deposited on TiO_2 P25 via a conventional impregnation−reduction method, and the resulting composite was hydrogenated in a H_2/N_2 flow under ambient atmosphere, at various temperatures (200−700 °C). The authors found that TiO_2 reduction and blackening occurred during annealing via "spillover", that is, H_2 gas dissociates at the Pt NP surface into H atoms that diffused, at a suitable temperature, into the TiO_2 lattice. This generated localized Ti−O(H)-Ti species that, upon dehydration of the oxide nanocrystals, converted into a substoichiometric form of TiO_2, that is, Ti_3O_5, which showed markedly higher H_2 generation rate (7.7 mmol h^{-1} g_{cat}^{-1}) compared with powders first hydrogenated and then loaded with Pt NPs.

The authors ascribed the photocatalytic enhancement to the strong visible light absorption of Ti_3O_5 powders. This widely

DOI: 10.1021/acscatal.8b04068
ACS Catal. 2019, 9, 345−364

reported assumption, particularly in the context of this study, appears however as a point of contradiction: among powders prepared under different experimental conditions (e.g., various temperatures or sequence of Pt deposition and hydrogenation), some samples showed virtually identical optical features (enhanced light absorption in the 400−800 nm range) but significantly different photocatalytic performances.[126]

Is then the improvement of visible light absorption crucial toward efficient solar photocatalysis? A picture of data in the literature reveals that often black TiO_2 presents a clear mismatch between enhanced optical properties and photocatalytic activity under visible-NIR illumination. Factors other than band gap narrowing and optical feature enhancement should therefore be taken into account to identify the origins of the activity improvement. This discrepancy was highlighted in follow-up works.[30,35,39,56,127]

Naldoni and co-workers[24] investigated the localization of defects of different nature within or at the surface of black TiO_2 nanocrystals. In their work, a high-surface-area ($\geq$500 m^2 g^{-1}) amorphous white TiO_2 powder was chosen as a precursor. Black TiO_2 was produced by annealing the amorphous powder at 500 °C under a pure H_2 stream at ambient pressure, followed by a fast cooling step to room temperature in an inert environment.

When treated under these conditions, the black TiO_2 nanocrystals featured a core−shell morphology with a ∼ 1.5 nm thick disordered surface layer characterized by a relatively high density of V_Os. VB-XPS data showed that the main absorption onset was located at 0.6 eV, whereas the maximum energy associated with the VB tail was reported to blue-shift toward the vacuum level at about −0.3 eV (Figure 10a). The

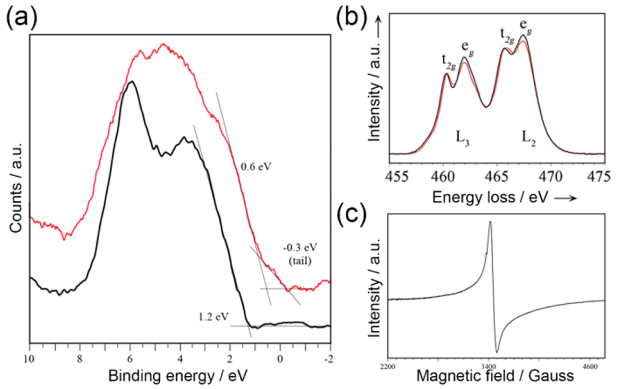

Figure 10. (a) VB-XPS spectra of P25 Degussa (black line) and black TiO_2 (red line). Thin black lines show the linear extrapolation of the curves used for deriving the band edge position of TiO_2 samples; (b) EELS spectra of the Ti $L_{2,3}$-edge for white (black line) and black (red line) TiO_2; (c) EPR spectra of black TiO_2 measured at 100 K. The strong EPR signal at about g = 1.957 is characteristic of paramagnetic Ti^{3+} centers. Reproduced from ref 56. Copyright 2012 American Chemical Society.

estimated E_g was 1.85 eV. Electron energy loss spectrum (EELS) analysis of the Ti $L_{2,3}$-edge was used to compare white and black TiO_2: the results revealed a ∼ 20% decrease of the t_{2g}-e_g splitting for the L_2 peak of black TiO_2 compared to white anatase (Figure 10b). This has been correlated to the formation in the crystal lattice of Ti^{3+} sites, which were also observed by EPR spectroscopy (Figure 10c).[114]

However, the absence of the superoxide radical (O_2^-) signal in the EPR spectra suggested that such Ti^{3+} centers are only present in the bulk (core) of the crystals and not at their surface. Therefore, the authors proposed the rapid cooling after hydrogenation to be a crucial step to "freeze" the metastable defective phase in the core of the nanocrystals; the Ti^{3+} rich core was responsible for the black coloration of the powders (i.e., Ti^{3+} are the color centers). So-formed black TiO_2 powders, however, showed activity for solar H_2 evolution only upon noble metal modification (with Pt or Au, reaching performances of 1.4−1.9 $mmol_{H_2}$ h^{-1} g_{cat}^{-1}), and the photocatalytic efficiency became negligible under visible light illumination (<10 μmol_{H_2} h^{-1} g_{cat}^{-1} with λ > 420 nm).[25] This work highlighted that a high number of bulk lattice defects is detrimental for the photocatalytic activity. Besides, Kong et al.[128] demonstrated, through positron annihilation experiments in reduced TiO_2, that a decrease of the ratio of bulk defects to surface defects could significantly improve the separation efficiency of photogenerated electrons and holes, which significantly enhanced the photocatalytic efficiency.

The reasons behind the inactivity of black TiO_2 are still under lively debate; however, plausible explanations are that (i) V_Os can introduce bandgap electronic states localized at 0.75−1.18 eV below the CB edge (i.e., below the redox potential for hydrogen evolution), which means that electrons photopromoted to such states are inactive for H_2 evolution;[120,129,130] and that (ii) defects in TiO_2 lattice can, when present in high concentration, act as recombination centers for photogenerated charge carriers.[121,122,130,131] These aspects will be discussed in detail below.

In contrast to "drastic" hydrogenation treatments (that typically form highly defective TiO_2 with strong visible light absorption), more refined hydrogenation approaches have been meanwhile developed.[115,116] In this context, research focus has shifted from the "mere" optical properties of TiO_2 to aspects such as the engineering of defects at the TiO_2 (sub)surface, the resulting electronic properties and stability, and the location and role of Ti^{3+} sites in photocatalysis.

Yang et al.[115] outlined an approach to produce rutile TiO_2 core−shell nanocrystals with a sulfided, disordered surface, having different colors from brown to black depending on the preparation conditions. The preparation implied a first step to reduce crystalline TiO_2 (anatase or rutile phase) with molten aluminum: Al powders and pristine TiO_2 were heated in vacuum in two distinct zones of a tubular furnace (Figure 11a). The Al zone was kept at 800 °C (i.e., molten Al), while TiO_2 was heated up to 500 °C. The pretreated TiO_2 nanopowders were then sulfided at 600 °C in a H_2S stream. The duration of the H_2S treatment was varied to introduce different S doping levels in TiO_2 and different light absorption properties (Figure 11b). By this approach, no Al impurities were introduced in the TiO_2 powders. The authors reported that regardless of the initial crystallinity of the TiO_2 precursor, the product was in any case composed of rutile TiO_2 phase; hence, it was proposed that in the presence of H_2S, the anatase-into-rutile phase transition may take place at temperature as low as 600 °C.[132]

The authors discussed also the morphological and crystallographic evolution observed when anatase powders were reduced and sulfided. They observed that upon reduction (Al-treatment), the entire core of the anatase nanocrystals was converted into rutile phase and the disordered surface layer became crystalline upon sulfidation. By contrast, only a minor surface reconstruction took place in rutile crystals, which after

DOI: 10.1021/acscatal.8b04068
ACS Catal. 2019, 9, 345−364

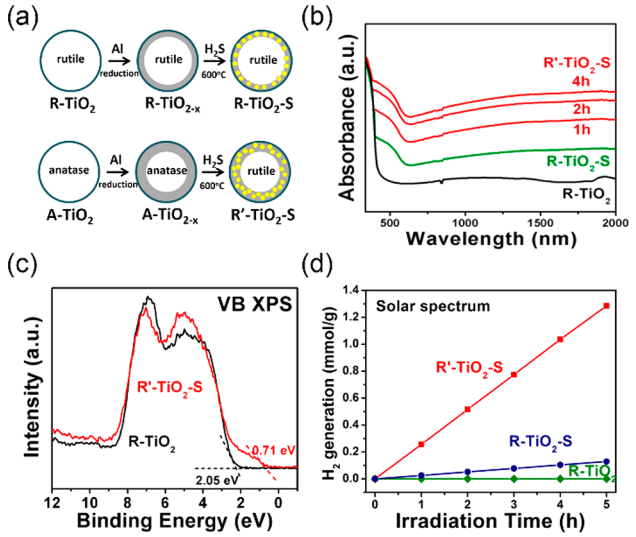

Figure 11. (a) Schematic synthetic routes to reduced rutile TiO_2 with sulfided disordered surface. (b) Diffuse reflectance spectra of reduced TiO_2 (R-TiO_2), reduced-sulfided rutile TiO_2 (R-TiO_2−S), and reduced-sulfided anatase TiO_2 (R′-TiO_2−S) with different sulfidation time. (c) VB XPS of representative samples. (d) Solar-driven water splitting for H_2 generation by investigated samples. Reproduced from ref 121. Copyright 2013 American Chemical Society.

reduction-sulfidation still exhibited the "disordered" shell. The authors reported that reduction and sulfidation (S-doping) induced a strong tailing of the anatase VB edge (as observed by VB XPS measurements), with consequent band gap narrowing (Figure 11c). On the basis of DFT calculations, it was suggested that surface defects and lattice reconstruction can introduce localized Ti^{3+} states below the CB minimum. The authors also claimed that Ti^{3+} paramagnetic signals (assigned to $O_2^{-\bullet}$ radicals ascribed to surface Ti^{3+} centers)[120,133] decreased in intensity with increasing the sulfidation time, and that sulfur accumulated at the particle surface (this is in our view not supported by the provided results), that is, the decrease of Ti^{3+} concentration is claimed to be caused by surface S^{2-} incorporation (substitution).

Compared with powders that were only Al-reduced, reduced-sulfided anatase was found to be significantly more active, leading to a H_2 evolution rate of ∼260 μmol h^{-1} g_{cat}^{-1} (Figure 11d); it is not clear however if such activity was measured under solar light or visible light illumination only. Besides, no evaluation of the stability of the photocatalytic performance was provided in this work, while photoanodes fabricated from such reduced-sulfided anatase were found in photoelectrochemical experiments to degrade under acidic and neutral pH conditions, and to deliver a clearly unstable photocurrent signal in alkaline electrolytes.

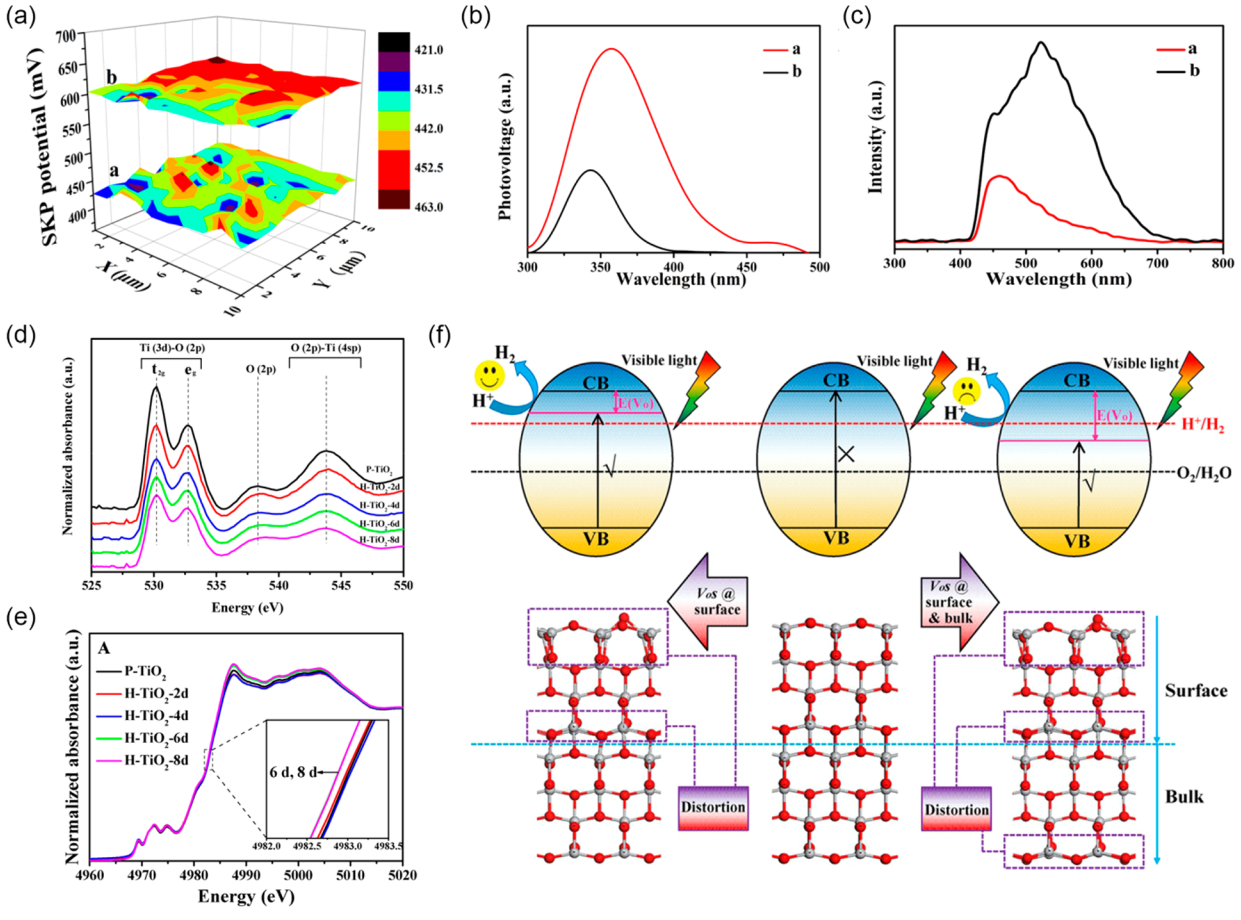

Figure 12. (a) Scanning Kelvin probe microscopy (SKPM) maps; (b) surface photovoltage spectroscopy (SPS) and (c) fluorescence spectra of white and black (hydrogenated) TiO_2 NTs. (d) O K-edge and (e) Ti K-edge XANES spectra (inset shows an enlarged view in the range from 4982.0 to 4983.5 eV) of untreated and hydrogenated anatase TiO_2 powders. (f) Schematic diagram of the changes in the electronic and band structure that occur upon hydrogenation. (a−c) Reproduced from ref 131. Copyright 2017 American Chemical Society; (d−f) Reproduced from ref 130. Copyright 2016 Wiley-VCH.

DOI: 10.1021/acscatal.8b04068
ACS Catal. 2019, 9, 345−364

Also, it was suggested that Ti^{3+} centers were responsible for the photocatalytic enhancement, but detailed reasons to support this assumption were not provided. Besides, the authors proposed that the concentration of surface Ti^{3+} centers is key to enable visible light activity, and the introduction of S^{2-} species in the highly defective surface of Al-treated TiO_2 allows to stabilize Ti^{3+} centers and to "adjust" their concentration.

Progresses in visible light photocatalytic performance were reported by Sinhamahapatra et al.,[122] who developed a TiO_2 reduction approach inspired by the Kroll process[134] (i.e., the reduction of $TiCl_4$ in the presence of Mg at high temperature to produce metallic Ti). Anatase TiO_2 was mixed with Mg powder and then treated in a tubular furnace at 650 °C in a H_2/Ar flow. After annealing, the reduced powders were washed in HCl to remove traces of Mg. "Differently reduced" TiO_2 samples were obtained by a stepwise increase of Mg loading, and the reduced anatase powders exhibited a gradually darker color (light gray, gray, pale blue, dark blue, black). The authors found that the concentration of V_Os and Ti^{3+} centers and the visible light absorbance of the powders were correlated, and both increased with darkening of the powders.

When testing these photocatalysts (after surface decoration with Pt NPs), the H_2 generation increased accordingly to the amount of Mg up to a certain Mg loading and then dramatically decreased, reaching performances comparable to those of untreated samples; that is, the most active photocatalyst was "only mildly reduced", appeared pale blue in color (not black!), and delivered a H_2 generation rate under visible light of ~440 μmol h^{-1} $g_{cat}{}^{-1}$, which was even higher than that of reduced-sulfided black rutile powders.[115] Such pale blue powders, compared to samples reduced to either lower or higher degrees, exhibited the lowest photoluminescence intensity, corresponding to a limited radiative charge recombination. The authors proposed that controlled "doses" of Ti^{3+} surface centers can on the one side enable visible light absorbance and on the other side provide a more efficient charge separation, thereby enhancing the overall photocatalytic performance under solar light.[116]

A similar interpretation was provided by Zhang et al.[131] In their work, black TiO_2 nanotubes with a mesoporous nanosheet architecture of the walls were synthesized by a solvothermal method, combined with an ethylene diamine surface modification step to protect the mesoporous framework from collapsing during hydrogenation (ethylene diamine is also reported to prevent the anatase-into-rutile phase transition). After synthesis, the powders were annealed at 600 °C in hydrogen and then loaded with Pt NPs. A combination of different techniques was used to characterize the powders and the results overall fit to previous literature:[24,90] as commonly reported, the blackened samples absorb visible light, owing to a tailing of the CB and consequent band gap narrowing; the CB tailing is ascribed to the formation of V_Os and Ti^{3+} centers upon hydrogenation.

In the photocatalytic tests, the Pt-modified black nanotubes were more active for H_2 generation compared with white structures, both under UV and visible light illumination, and their H_2 generation rate was ~200 μmol h^{-1} $g_{cat}{}^{-1}$ for $\lambda > 420$ nm. Scanning Kelvin probe (SKP) microscopy (Figure 12a) revealed that for hydrogenated TiO_2 NTs, the work function decreases from ~5.71 eV to ~5.54 eV; that is, TiO_2 reduction led to an upward shift of the oxide Fermi level. Surface photovoltage spectroscopy (SPS) featured for both black and white NTs a peak at around 350 nm that could be attributed to the electron transitions from the VB to the CB (band-to-band transitions, O_{2p}-Ti_{3d}) associated with UV light absorption, but the built-in photovoltage was significantly higher for black NTs, which also featured a red-shifted photovoltage onset at ~500 nm (Figure 12b).

The fluorescence intensity of black NTs was found to be lower than that of white powders (Figure 12c), hence corroborating the enhanced separation efficiency of photogenerated charge carriers. Based on their results, the author interpretation was that for black TiO_2 NTs the presence of defects (V_Os and Ti^{3+}) and the consequently higher density of free charge carriers can modify the built-in electric field: the upward shift of the Fermi level was addressed as a main cause for the photocatalytic enhancement, as it could lead to a more pronounced surface band bending that enables a kinetically favored (accelerated) transfer of photogenerated electrons to the Pt cocatalyst for H_2 evolution.

More recently, Xue et al.[130] explored the nature of CB tailing in hydrogenated TiO_2 and proposed a plausible interpretation of the origin of visible light activity. In this study, reduced TiO_2 NPs were obtained by heating hydrothermal anatase TiO_2 nanoparticles in a H_2 flow at 200 °C for periods of time ranging from 2 to 8 days. Then, Pt was loaded as cocatalyst prior to the photocatalytic tests. Depending on the duration of the H_2-treatment, the white TiO_2 precursor was found to turn into powders of gradually darker colors. The authors aimed at investigating the nature of the defects introduced in the oxide with the aid of surface sensitive soft X-ray techniques, hard X-ray techniques, and EPR spectroscopy; the distortion of the TiO_2 lattice consequent to hydrogenation was modeled by means of EXAFS results and DFT calculations.

Powders hydrogenated up to 4 days were characterized by an EPR signal that can be associated with surface Ti^{3+} states, while a different EPR signature, which is typical of bulk Ti^{3+}, appeared for longer hydrogenation treatments.[130] Besides, the authors claimed that surface sensitive XANES analysis revealed that the O K-edge signal varies only at the beginning of the hydrogenation process (Figure 12d), while bulk measurements evidenced that the Ti K-edge was different only for long H_2 treatment (>4 days, Figure 12e)—in our view, these data seem not to be fully convincing as one can hardly appreciate any trend aside from for hydrogenation times ≥6 days). However, the authors reported that EXAFS analysis of the radial structure functions (RSFs) showed that distortions of the lattice (i.e., the variation of the interatomic distances with respect to the regular TiO_2 octahedral symmetry) occurred only at the surface or both at the surface and in the bulk of the structure with short or long hydrogenation treatments, respectively.

These changes appeared to correlate to the photocatalytic performance, as gray TiO_2 powders produced by an "intermediate" reduction treatment showed the highest visible light activity. Thus, the authors inferred that an explanation to these findings (Figure 12f) could be derived from DFT calculations based on XANES and EXAFS results, in relation to the density and location of V_Os, and their consequences on the extent of tailing of TiO_2 CB. In their interpretation, the authors proposed that at the beginning of hydrogenation, V_Os are generated at the surface of TiO_2, which leads to a small tail of the CB owing to a relatively low V_O density. The energy level of such V_Os is still above the H^+/H_2 redox potential; the induced modified electronic structure enables visible light

DOI: 10.1021/acscatal.8b04068
ACS Catal. 2019, 9, 345−364

absorption that generates electron with adequate thermodynamic driving force to contribute to H_2 evolution even for $\lambda >$ 420 nm. Upon increasing the hydrogenation time, the CB tailing tends to further extend toward the H^+/H_2 redox potential because of the increase of V_O states. The light absorption onset meanwhile shifts to longer wavelength, and electrons photopromoted to these V_O states still have a sufficiently high potential to generate H_2. This could explain the enhancement of visible light activity. On the contrary, at a high "degree" of hydrogenation, a high density of V_Os may be generated, which locate not only at the surface but also in the bulk of the TiO_2 crystals. As a consequence, the tail of the CB can extend below the H^+/H_2 redox potential. In this situation, the absorption of visible light is enhanced, and under solar illumination more electrons can be excited to the CB, but a substantial part of them cannot contribute to H_2 evolution. This would explain why an excessive enhancement in the visible light absorption has more likely a negative effect on the photocatalytic H_2 evolution rate of black TiO_2 nanomaterials.

4.2. Cocatalyst-Free TiO_2 Photocatalysts. Greatest challenges in using TiO_2 for photocatalysis are the large bandgap (allowing only for UV light activation) and the significant charge carrier recombination.

As discussed above, different reduction approaches have been explored to form "colored" TiO_2 by shifting its absorption onset toward the visible range. On the other hand, charge recombination and therefore the sluggish kinetics of charge carrier transfer is usually tackled by decorating TiO_2 with noble metal cocatalysts such as Pt, Pd, Au, nanoparticles,[135,136] or, more recently, with non-noble elements or element combinations (e.g., alloys).[137] Metal cocatalyst NPs enable significant H_2 evolution rates by efficiently separate electrons and hole through a Schottky barrier formation at the interface with TiO_2, and by acting as catalytic centers for hydrogen production.[135,136,138]

Noble metals (particularly Pt) are typically more active than their non-noble counterparts; indeed, by contrast, their adoption questions the economic benefit of using low-cost TiO_2-based photocatalysts. Thus, remarkable is in this context another property of hydrogenated TiO_2 that has been reported by Liu et al. and others,[35,37,132] that is, hydrogenated or reduced TiO_2 in different morphologies (e.g., anodic nanotubes,[39,127,139] powders,[89,132] single crystals[140]) is able to photocatalytically generate H_2 in the absence of any noble metal cocatalyst, owing to the formation of intrinsic cocatalytic sites. It is worth mentioning that this feature has been overlooked in previous works as the enhanced photocatalytic activity of black TiO_2 has been in almost every report solely ascribed to optical properties and to the formation of an amorphous shell encapsulating the TiO_2 particles and by using cocatalysts.

This unique cocatalytic effect has been observed for example for TiO_2 anatase NPs treated with H_2 under high pressure; the treatment can activate a strong and stable photocatalytic H_2 evolution in commercial anatase or in mixed anatase/rutile nanoparticles. However, no significant activation was found when conventional reduction processes, for example, annealing in Ar, were used for treating various TiO_2 polymorphs (Figure 13a). Also, this activation was not observed when pure rutile powders were hydrogenated.[132]

Typically, the activation can be enabled for TiO_2 powders (anatase or mixed anatase−rutile phase) via hydrogenation in pure H_2, at, for example, 500 °C, at 20 bar, for durations of the

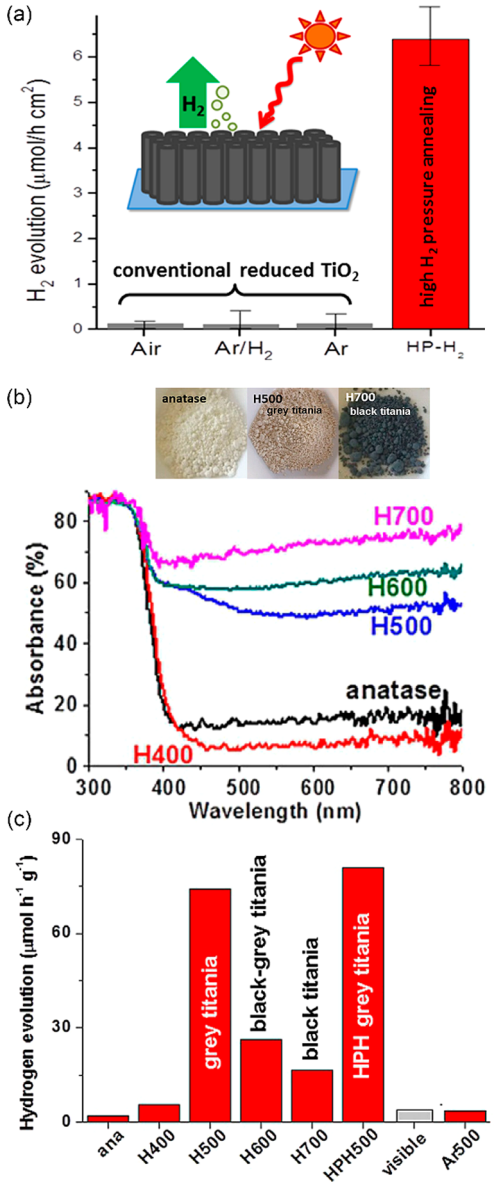

Figure 13. (a) Photocatalytic H_2 production measured under open circuit conditions in methanol/water (50/50 vol %) under AM1.5 (100 mW cm^{-2}) illumination with anodic TiO_2 nanotubes treated in different atmospheres; Air: heat treatment in air at 450 °C; Ar: heat treatment in pure argon at 500 °C; Ar/H_2: heat treatment in H_2/Ar (5 vol %) at 500 °C; HP-H_2: heat treatment in H_2 at 20 bar and 500 °C; (b) Optical images of anatase nanopowders untreated ("anatase") and treated ("H500" and "H700") under different hydrogenation conditions ("H500" and "H700" stand for heat treatment in H_2 at 20 bar at 500 and 700 °C, respectively), and relative integrated light reflectance spectra; (c) Photocatalytic hydrogen evolution rate under AM 1.5 illumination (100 mW cm^{-2}) for TiO_2 nanoparticles after different hydrogenation treatments, a reference treated in argon gas at 500 °C, and the most active sample if UV light is blocked (visible light only). (a) Reproduced from ref 139. Copyright 2014 American Chemical Society. (b,c) Reproduced from ref 29. Copyright 2016 Wiley-VCH.

treatment between few hours to some days, reaching solar H_2 evolution rates of >200 μmol h^{-1} $g_{cat}{}^{-1}$.[132] Also TiO_2 nanotubes were active for H_2 generation in the absence of a cocatalyst when treated under similar conditions, enabling solar H_2 evolution with rates of ~6 μmol h^{-1} cm^{-2}.[35] Liu et al.

DOI: 10.1021/acscatal.8b04068
ACS Catal. 2019, 9, 345−364

demonstrated that hydrogenated anatase TiO_2 powders or nanotubes did not undergo substantial morphological changes, for example, "amorphization" effects forming crystalline−amorphous core−shell structures, and the hydrogenated structures generally maintained their crystalline nature. However, some minor modifications were observed (by TEM analysis), i.e., voids that form inside the particles (or in the nanocrystals composing the polycrystalline NT walls). This has been explained in terms of either internal formation of gas bubbles, or more likely, due to vacancy clustering.[30,141,142]

A crucial finding in the work of Liu et al. is that, in view of noble metal-free H_2 evolution on anatase TiO_2 powders, the activity showed a maximum efficiency at intermediate reduction treatments, that is, highly reduced black TiO_2 showed (in the absence of cocatalyst) a suboptimum efficiency, which is in stark opposition to earlier reports.[89]

Liu and co-workers[116] reported that for anatase powders subjected to different "degrees" of hydrogenation (Figure 13b), gray specimens were significantly more active than fully blackened counterparts (Figure 13c). Strikingly, the illumination of any of these samples with visible light ($\lambda \sim 420$ nm) did not produce measurable amounts of H_2; also, when doctor-blading these powders on FTO slides to be used as photoanodes in a photoelectrochemical (PEC) setup, no photocurrent could be registered under visible light illumination, and photocurrent spectra revealed in any case a band gap $E_g \sim 3.2$ eV, corresponding to the typical E_g of TiO_2 anatase phase. It was proposed, in other words, that the materials' intrinsic activity for photocatalytic hydrogen evolution was not coupled with their visible light absorption behavior, but was rather ascribed to an optimized formation of a "specific" type of defect.

In this regard, hydrogenated cocatalyst-free active TiO_2 powders and NTs, because of their specific electronic properties, exhibit some common "fingerprints" in EPR and PL spectroscopy that can be considered key indicators for their activity. For example, compared with EPR results for untreated TiO_2, or treated by conventional reduction processes (Ar), the characteristic EPR signature of high-temperature high-pressure hydrogenated TiO_2 NTs featured (at 4K) a strong signal corresponding to Ti^{3+},[143] while the signal assigned to the V_Os was comparably small. Even more marked differences have been observed in spectra recorded at room temperature as the high-pressure treated material still exhibited a distinct signature of Ti^{3+}, apparent as separated lines and indicating the presence of isolated surface Ti^{3+} centers,[144] whereas that of Ar-annealed nanotubes typically fades off.[35] On the other hand, black TiO_2, which shows no (or comparably lower) cocatalyst-free H_2 generation activity, exhibited very strong paramagnetic signals typical of Ti^{3+}/V_O centers introduced in high concentration into the TiO_2 lattice.[29,145,146]

Characteristic electronic features of H_2-treated anatase can also be distinguished by PL; typical for the gray powders is the appearance of a peak at ∼400−450 nm that can be associated with transitions from a sub-bandgap defect state to the CB. Based on PL results, it was derived that defects would have to be located energetically close to the CB, that is, at $\Delta E \sim 0.2$−0.5 eV, which is significantly closer than $\Delta E \sim 0.8$−1.2 eV below the CB reported for typical Ti^{3+} states formed by conventional reduction approaches.[145,147,148]

On the basis of these findings and the results of various other complementary physicochemical characterization techniques, it has been inferred that the cocatalyst-free photocatalytic H_2 evolution activity of hydrogenated TiO_2 originated from stabilized Ti^{3+} states that are energetically close to the CB of TiO_2. Such intrinsic Ti^{3+} active centers were undetectable by XPS.[35,132] In contrast, inactive (and unstable) Ti^{3+} species generated by Ar ion bombardment typically produce a clear Ti^{3+} XPS signal (when generated under vacuum conditions and directly detected without exposure to the environment).[35,149] The difference in the nature of these defects lies on the one hand in their different energetic level within the bandgap of TiO_2 (this explains their intrinsic activity or inactivity), and on the other hand in their different location and configuration, as observed, for example, in single crystals of different TiO_2 polymorphs. For instance, in anatase single crystals, photocatalytically active Ti^{3+} centers may be generated and stabilized in a subsurface configuration. However, this cocatalytic activation, in order to translate into an observable cocatalyst-free H_2 evolution activity, was found to require the presence of defects (high index places), which do not occur on single crystal low index planes of anatase, but could nevertheless be artificially introduced by simple scratching (with a diamond scriber) or by ion implantation damage.[140] Differently, comparable hydrogenation treatments applied to rutile single crystals generated V_Os that tend to remain segregated at the surface,[34,99] and this difference has been found to substantially alter the defect reactivity for the two polymorphs. This may also explain why activation through hydrogen treatment was not observed for pure rutile powders.[89,147]

Follow-up work demonstrated that similarly active cocatalytic centers can be introduced by alternative approaches.[36,39,40,51,150,151] For example, high-energy proton ion-implantation was used to modify TiO_2 nanotubes selectively at their tops, and in the proton-implanted region, the creation of such intrinsic cocatalytic sites was observed, which were active for photocatalytic H_2 evolution. Proton implantation can induce specific defects and a characteristic modification of the electronic properties not only in nanotubes but also in anatase single crystal (001) surfaces (reaching cocatalyst-free solar H_2 evolution rates of ∼15 and ∼0.2 μmol h^{-1} cm^{-2}, respectively). The extent of activation (relative increase of H_2 evolution rate) was found to be much higher for the nanotubes; this result was explained by proposing a synergetic effect between the implanted region (that behaves as the catalytic zone) and the implant-free tube segment underneath (that acts as light absorber and charge carrier generator).[39,151]

Milling TiO_2 with TiH_2 powders was also found to provide a strong enhancement of the photocatalytic H_2 generation in the absence of cocatalyst. A systematic parameter screening revealed that both ball milling duration as well as TiH_2 loading strongly affected the photocatalytic H_2 generation, and both led at a lower magnitude to a beneficial effect but become detrimental at a higher magnitude.

Interestingly, powders milled under optimize conditions show H_2 evolution rates (∼220 μmol h^{-1} g^{-1}) that were comparable with the activation reached by high pressure hydrogenation treatments and/or H-ion implantation.[132,134]

In this sense, Zhang et al.[37] reported, to the best of our knowledge, the highest solar H_2 evolution efficiency for TiO_2 under cocatalyst-free conditions. In their work, Degussa P25 TiO_2 nanoparticles were treated at room temperature in a reducing medium prepared by dissolving Li in ethylene diamine (EDA). The treatment selectively attacks (i.e.,

DOI: 10.1021/acscatal.8b04068
ACS Catal. 2019, 9, 345−364

reduces) the rutile phase, this because of a large difference in the protonation constants between rutile and anatase, while anatase domains were left unaltered. The result was a blue TiO_2 powder composed of particles that feature nanosized, adjacent domains (junctions) of crystalline anatase and amorphous (protonated) rutile (Figure 14a–e). Such powders

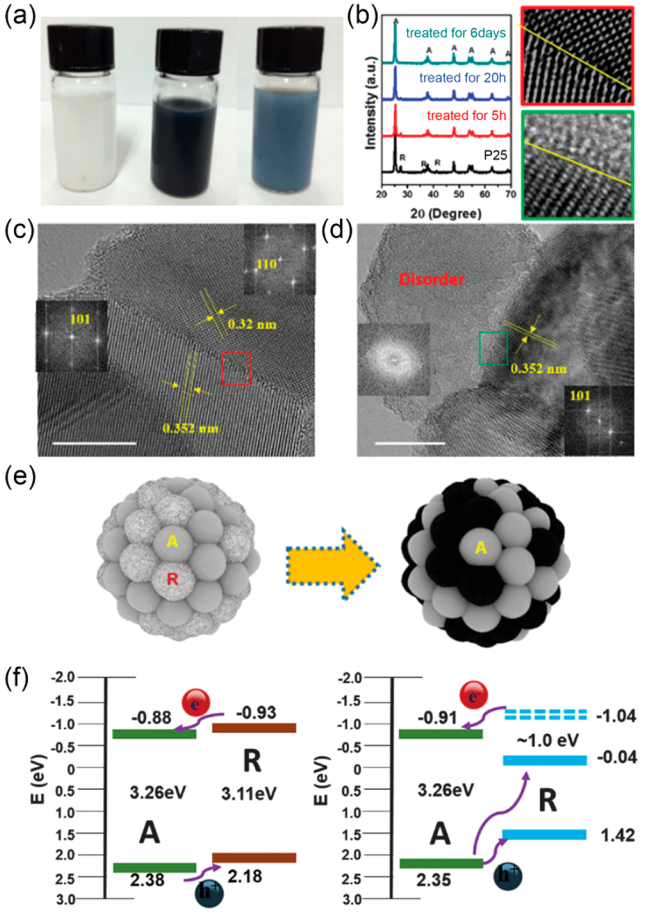

Figure 14. (a) Photographs of anatase TiO_2 (A-TiO_2, left), rutile TiO_2 (R-TiO_2, middle) and blue P25 (right) suspensions (0.05 g L^{-1}) after Li-EDA treatment for 6 days; (b) XRD patterns of the Li-EDA-treated P25 crystals with different treatment times; A = anatase phase and the R = rutile phase; (c) HR-TEM images and SAED patterns of P25; scale bar = 10 nm; (d) HR-TEM images and SAED pattern of blue P25; scale bar = 10 nm. Insets: enlarged TEM images taken on the junction area (red squares: P25, and green squares: blue P25); (e) Schematic of the P25 (left) and blue P25 crystals (right). The black color corresponds to the visual color of the reduced R-TiO_2; (f) Calculated bandgap diagrams created by combining UV–vis absorption and VB XPS spectra. Reproduced from ref 37. Copyright 2016 The Royal Society of Chemistry.

led, in the absence of any cocatalyst, to a H_2 evolution rate of ~3.5 mmol h^{-1} g_{cat}^{-1}, which is at least 1 order of magnitude higher than most of the data in the literature. Band diagrams, drawn according to optical and VB XPS measurements, and corroborated by DFT simulations, suggested that for treated P25 the energetic situation at the junction between crystalline anatase and amorphous rutile domains deviated substantially from that of as-purchased P25,[152] that is, the Li-treatment generated a "type II" semiconductor heterojunction, due to Ti^{3+} and V_Os formation in the rutile phase and consequent changes in its electronic structure (see Figure 14f). On the basis of these considerations and of the results of time-correlated single-photon counting (TCSPC) and low-temperature PL measurements, the authors proposed that a main reason for the highly improved cocatalyst-free H_2 evolution activity is the charge separation across the crystalline anatase/disordered rutile interface, which can substantially suppress the electron–hole recombination. As an additional reason, the authors also inferred that, in this configuration, the photocatalytic "cathodic" and "anodic" reactions (H_2 generation and methanol mineralization) are spatially confined at the surface of the crystalline anatase and disordered rutile domains, respectively, and both domains are exposed to the water phase (Figure 14e,f). This means that charge transfer to the environment is not hampered, whereas it is, in principle, in "ordered-disordered" core–shell structures typically formed by hydrogenation treatments, where charges formed in the crystalline bulk must diffuse across the amorphous shell to reach the environment (this would explain the higher activity of Li-treated P25 compared to hydrogenated counterparts). It is also worthwhile to mention that the apparent quantum efficiency measured for blue P25 under visible light illumination (λ > 420 nm) was negligible, and the authors concluded that the intense, broad background absorption seen at wavelengths longer than 400 nm (associated with the blue-shifted band tail) cannot be the origin of the photoactivity.

5. CONCLUSIONS AND OUTLOOK

In this Review, we have provided an overview of the progress made in photocatalytic hydrogen generation with reduced TiO_2, bringing to the attention many aspects of defective oxides that are usually overlooked and should be explored more thoroughly to further develop hydrogenated TiO_2 performance.

Hydrogenation treatments (carried out under various conditions) have been demonstrated to lead to colored forms of TiO_2 that exhibit strong visible and NIR light absorption.

As a "rule of thumb", the darker is the color, the higher is the light absorption ability, with "black TiO_2" showing the most intense visible light absorbance. Hydrogenation (and other means of reduction) can also create, under optimized conditions, variations of "gray TiO_2" that feature intrinsic cocatalytic active centers similar to the cocatalytic effect obtained by noble metal cocatalyst decoration. Most of the reports on hydrogenated TiO_2 for photocatalytic H_2 generation, and particularly those on "black" TiO_2, have however used noble metal cocatalysts when measuring the solar H_2 evolution activity. Thus, despite the seeming connection of the two effects (visible light absorption vs intrinsic cocatalytic activation), it still remains questionable whether the enhanced visible-light absorption is indeed mechanistically coupled to the photocatalytic activity in cocatalyst-free hydrogen evolution.

The intense research in the field has meanwhile led to a tremendous progress in solar photocatalytic efficiencies. A picture of such progress becomes clear if one takes into account that solar H_2 evolution rates of benchmark Pt-TiO_2 photocatalysts are typically ~41 mmol h^{-1} g_{cat}^{-1},[153] that of Pt-decorated reduced TiO_2 (with a comparable Pt cocatalyst loading) has reached ~43 mmol h^{-1} g_{cat}^{-1},[122] and that of cocatalyst-free hydrogenated TiO_2 has been pushed up to ~3.5 mmol h^{-1} g_{cat}^{-1}.[37] Solar-active cocatalyst-free TiO_2 photocatalysts, however, seem to still suffer from a substantial visible-

DOI: 10.1021/acscatal.8b04068
ACS Catal. 2019, 9, 345–364

light inactivity (or suboptimum activity); that is, hydrogenation and reduction treatments apparently aid mainly to a more efficient use of UV light photons, while effective and reliable means to boost TiO_2 activity driven purely by visible light have yet to be developed. Hence, in view of a sustainable, noble-metal-free solar photocatalytic H_2 generation the gap to fill to reach "reasonable" efficiencies is still wide.

To reach cocatalyst-free efficiency comparable to noble-metal modified TiO_2, several research questions must be answered, and fundamental studies must be undertaken to unveil the elusive understanding that we still have on reduced TiO_2 nanomaterials.

First, a precise description of the structure and electronic signatures of defective cocatalytic sites forming upon reduction must be provided, taking advantage from previous surface science and model studies on TiO_2 single crystals. In particular, an effective strategy to distinguish the presence of defects pairing and clustering of defects is still elusive, while it might bring exciting results both in terms of light absorption capabilities (i.e., selective light absorption) and chemical activation toward common substrates used in photocatalytic water splitting and photoreforming of alcohols. In this regard, high resolution X-ray spectroscopies may provide valuable information on defective sites, while mapping techniques such as atom probe tomography and aberration-corrected high-resolution transmission electron microscopy may provide hints on structural organization of reduced TiO_2.

In contrast, operando experiments (i.e., in liquids under light illumination) with EPR, infrared, and X-ray spectroscopies are foreseen to provide crucial information on the behavior and reactivity of unpaired electrons during photocatalytic hydrogen generation.

The development of new materials for cocatalyst-free hydrogen evolution is also strictly related to the development of alternative methodologies for synthesizing mildly reduced TiO_2, as opposed to the harsh synthesis conditions that are currently mostly utilized.

Another leap toward higher efficiencies might be provided if photocatalysis with reduced TiO_2 would be treated at the same way as heterogeneous catalytic systems, that is, following general precepts that constitute the foundations of heterogeneous catalysis. For instance, the reactivity of subsurface defects toward the activation of rate determining photocatalytic steps should be taken into account. In addition, the specific number of cocatalytic sites formed in partly reduced TiO_2 must be retrieved, making the computing of turnover frequency and turnover number possible. This would allow benchmarking the photocatalytic activity of different reduced TiO_2 nanomaterials reported in the literature and rationalize their structure−activity relationships.

Finally, another possible approach to increase the cocatalyst-free activity of reduced TiO_2 might come from the usage of different polymorphs rather than anatase and rutile. This might be obtained by engineering precise nanojunctions of reduced TiO_2 and exploring the reduction of brookite, the TiO_2 polymorph featuring the highest conduction band energy levels and holding great potential for hydrogen evolution. The challenge here is envisioned to stand in the poor stability of brookite when subjected to drastic hydrogenation or reduction treatments.

This entire set of tools, comprising defect engineering, design of nanojunctions, and use of advanced characterization techniques, will provide inspiration for finding new strategies to increase the understanding on the role of defects in TiO_2 to finally reach high photocatalytic activities for hydrogen production without the use of critical raw materials. Eventually, it may enable development of new clean energy technologies that might see light in future years.

AUTHOR INFORMATION

Corresponding Authors

*E-mail: alberto.naldoni@upol.cz.
*E-mail: schmuki@ww.uni-erlangen.de.

ORCID

Alberto Naldoni: 0000-0001-5932-2125
Marco Altomare: 0000-0002-7237-8809
Giorgio Zoppellaro: 0000-0003-2304-2564
Radek Zbořil: 0000-0002-3147-2196
Patrik Schmuki: 0000-0002-9208-5771

Author Contributions

The manuscript was written through contributions of all authors. All authors have given approval to the final version of the manuscript.

Notes

The authors declare no competing financial interest.

ACKNOWLEDGMENTS

The authors gratefully acknowledge the support by the Operational Programme Research, Development and Education—European Regional Development Fund, projects no. CZ.02.1.01/0.0/0.0/15_003/0000416 and CZ.02.1.01/0.0/0.0/16_019/0000754 of the Ministry of Education, Youth and Sports of the Czech Republic. M.A., N.L., and P.S. acknowledge ERC, DFG, and the DFG cluster of excellence EAM for financial support.

REFERENCES

(1) Lewis, N. S. Toward Cost-Effective Solar Energy Use. *Science* **2007**, *315*, 798−801.
(2) Lewis, N. S.; Nocera, D. G. Powering the Planet: Chemical Challenges in Solar Energy Utilization. *Proc. Natl. Acad. Sci. U. S. A.* **2006**, *103*, 15729−15735.
(3) Shaner, M. R.; Atwater, H. A.; Lewis, N. S.; McFarland, E. W. A Comparative Technoeconomic Analysis of Renewable Hydrogen Production Using Solar Energy. *Energy Environ. Sci.* **2016**, *9*, 2354−2371.
(4) Esposito, D. V. Membraneless Electrolyzers for Low-cost Hydrogen Production in a Renewable Energy Future. *Joule* **2017**, *1*, 651−658.
(5) Goto, Y.; Hisatomi, T.; Wang, Q.; Higashi, T.; Ishikiriyama, K.; Maeda, T.; Sakata, Y.; Okunaka, S.; Tokudome, H.; Katayama, M.; Akiyama, S.; Nishiyama, H.; Inoue, Y.; Takewaki, T.; Setoyama, T.; Minegishi, T.; Takata, T.; Yamada, T.; Domen, K. A Particulate Photocatalyst Water-splitting Panel for Large-scale Solar Hydrogen Generation. *Joule* **2018**, *2*, 509−520.
(6) Hisatomi, T.; Kubota, J.; Domen, K. Recent Advances in Semiconductors for Photocatalytic and Photoelectrochemical Water Splitting. *Chem. Soc. Rev.* **2014**, *43*, 7520−7535.
(7) Christoforidis, K. C.; Fornasiero, P. Photocatalytic Hydrogen Production: A Rift into the Future Energy Supply. *ChemCatChem* **2017**, *9*, 1523−1544.
(8) Fujishima, A.; Zhang, X.; Tryk, D. A. TiO_2 Photocatalysis and Related Surface Phenomena. *Surf. Sci. Rep.* **2008**, *63*, 515−582.
(9) Linsebigler, A. L.; Lu, G.; Yates, J. T. Photocatalysis on TiO_2 Surfaces: Principles, Mechanisms, and Selected Results. *Chem. Rev.* **1995**, *95*, 735−758.

DOI: 10.1021/acscatal.8b04068
ACS Catal. 2019, 9, 345−364

(10) Schneider, J.; Matsuoka, M.; Takeuchi, M.; Zhang, J.; Horiuchi, Y.; Anpo, M.; Bahnemann, D. W. Understanding TiO_2 Photocatalysis: Mechanisms and Materials. *Chem. Rev.* **2014**, *114*, 9919−9986.
(11) Nakanishi, H.; Iizuka, K.; Takayama, T.; Iwase, A.; Kudo, A. Highly Active $NaTaO_3$-Based Photocatalysts for CO_2 Reduction to Form CO Using Water as the Electron Donor. *ChemSusChem* **2017**, *10*, 112−118.
(12) Kuehnel, M. F.; Orchard, K. L.; Dalle, K. E.; Reisner, E. Selective Photocatalytic CO_2 Reduction in Water through Anchoring of a Molecular Ni Catalyst on CdS Nanocrystals. *J. Am. Chem. Soc.* **2017**, *139*, 7217−7223.
(13) Chen, X.; Li, N.; Kong, Z.; Ong, W.-J.; Zhao, X. Photocatalytic Fixation of Nitrogen to Ammonia: State-of-the-art Advancements and Future Prospects. *Mater. Horiz.* **2018**, *5*, 9−27.
(14) Cargnello, M.; Montini, T.; Smolin, S. Y.; Priebe, J. B.; Jaén, J. J. D.; Doan-Nguyen, V. V. T.; McKay, I. S.; Schwalbe, J. A.; Pohl, M.-M.; Gordon, T. R.; Lu, Y.; Baxter, J. B.; Brückner, A.; Fornasiero, P.; Murray, C. B. Engineering Titania Nanostructure to Tune and Improve Its Photocatalytic Activity. *Proc. Natl. Acad. Sci. U. S. A.* **2016**, *113*, 3966−3971.
(15) Chen, X.; Shen, S.; Guo, L.; Mao, S. S. Semiconductor-based Photocatalytic Hydrogen Generation. *Chem. Rev.* **2010**, *110*, 6503−6570.
(16) Chen, X.; Mao, S. S. Titanium Dioxide Nanomaterials: Synthesis, Properties, Modifications, and Applications. *Chem. Rev.* **2007**, *107*, 2891−2959.
(17) Asahi, R.; Morikawa, T.; Ohwaki, T.; Aoki, K.; Taga, Y. Visible-light Photocatalysis in Nitrogen-doped Titanium Oxides. *Science* **2001**, *293*, 269−271.
(18) Murphy, A. B. Does Carbon Doping of TiO_2 Allow Water Splitting in Visible Light? Comments on "Nanotube Enhanced Photoresponse of Carbon Modified (CM)-*n*-TiO_2 for Efficient Water Splitting. *Sol. Energy Mater. Sol. Cells* **2008**, *92*, 363−367.
(19) Liu, G.; Yin, L.-C.; Wang, J.; Niu, P.; Zhen, C.; Xie, Y.; Cheng, H.-M. A Red Anatase TiO_2 Photocatalyst for Solar Energy Conversion. *Energy Environ. Sci.* **2012**, *5*, 9603−9610.
(20) Zhao, J.; Zhang, L.; Xing, W.; Lu, K. A Novel Method to Prepare B/N Codoped Anatase TiO_2. *J. Phys. Chem. C* **2015**, *119*, 7732−7737.
(21) Tian, L.; Xu, J.; Alnafisah, A.; Wang, R.; Tan, X.; Oyler, N. A.; Liu, L.; Chen, X. A Novel Green TiO_2 Photocatalyst with a Surface Charge-transfer Complex of Ti and Hydrazine Groups. *Chem. - Eur. J.* **2017**, *23*, 5345−5351.
(22) Chen, X.; Liu, L.; Huang, F. Black Titanium Dioxide (TiO_2) Nanomaterials. *Chem. Soc. Rev.* **2015**, *44*, 1861−1885.
(23) Cronemeyer, D. C. Electrical and Optical Properties of Rutile Single Crystals. *Phys. Rev.* **1952**, *87*, 876−886.
(24) Cronemeyer, D. C.; Gilleo, M. A. The Optical Absorption and Photoconductivity of Rutile. *Phys. Rev.* **1951**, *82*, 975−976.
(25) Chen, X.; Liu, L.; Yu, P. Y.; Mao, S. S. Increasing Solar Absorption for Photocatalysis with Black Hydrogenated Titanium Dioxide Nanocrystals. *Science* **2011**, *331*, 746−750.
(26) Wang, B.; Shen, S.; Mao, S. S. Black TiO_2 for Solar Hydrogen Conversion. *J. Materiomics* **2017**, *3*, 96−111.
(27) Liu, X.; Zhu, G.; Wang, X.; Yuan, X.; Lin, T.; Huang, F. Progress in Black Titania: A New Material for Advanced Photocatalysis. *Adv. Energy Mater.* **2016**, *6*, 1600452.
(28) Fang, W.; Xing, M.; Zhang, J. Modifications on Reduced Titanium Dioxide Photocatalysts: A Review. *J. Photochem. Photobiol., C* **2017**, *32*, 21−39.
(29) Liu, N.; Zhou, X.; Nguyen, N. T.; Peters, K.; Zoller, F.; Hwang, I.; Schneider, C.; Miehlich, M. E.; Freitag, D.; Meyer, K.; Fattakhova-Rohlfing, D.; Schmuki, P. Black Magic in Gray Titania: Noble-metal-free Photocatalytic H_2 Evolution from Hydrogenated Anatase. *ChemSusChem* **2017**, *10*, 62−67.
(30) Liu, N.; Schneider, C.; Freitag, D.; Venkatesan, U.; Marthala, V. R. R.; Hartmann, M.; Winter, B.; Spiecker, E.; Osvet, A.; Zolnhofer, E. M.; Meyer, K.; Nakajima, T.; Zhou, X.; Schmuki, P. Hydrogenated Anatase: Strong Photocatalytic Dihydrogen Evolution without the Use of a Co-Catalyst. *Angew. Chem., Int. Ed.* **2014**, *53*, 14201−14205.
(31) Breckenridge, R. G.; Hosler, W. R. Titanium Dioxide Rectifiers. *J. Res. Natl. Bur. Stand.* **1952**, *49*, 65.
(32) Cronemeyer, D. C. Infrared Absorption of Reduced Rutile TiO_2 Single Crystals. *Phys. Rev.* **1959**, *113*, 1222−1226.
(33) Hollander, L. E., Jr. Piezoresistivity in Reduced Single-Crystal Rutile (TiO_2). *Phys. Rev. Lett.* **1958**, *1*, 370−371.
(34) Diebold, U. The Surface Science of Titanium Dioxide. *Surf. Sci. Rep.* **2003**, *48*, 53−229.
(35) Liu, N.; Schneider, C.; Freitag, D.; Hartmann, M.; Venkatesan, U.; Müller, J.; Spiecker, E.; Schmuki, P. Black TiO_2 Nanotubes: Cocatalyst-Free Open-Circuit Hydrogen Generation. *Nano Lett.* **2014**, *14*, 3309−3313.
(36) Wu, Q.; Huang, F.; Zhao, M.; Xu, J.; Zhou, J.; Wang, Y. Ultra-small Yellow Defective TiO_2 Nanoparticles for Co-catalyst Free Photocatalytic Hydrogen Production. *Nano Energy* **2016**, *24*, 63−71.
(37) Zhang, K.; Wang, L.; Kim, J. K.; Ma, M.; Veerappan, G.; Lee, C.-L.; Kong, K.-j.; Lee, H.; Park, J. H. An Order/Disorder/Water Junction System for Highly Efficient Co-catalyst-free Photocatalytic Hydrogen Generation. *Energy Environ. Sci.* **2016**, *9*, 499−503.
(38) Zhou, X.; Liu, N.; Schmidt, J.; Kahnt, A.; Osvet, A.; Romeis, S.; Zolnhofer, E. M.; Marthala, V. R. R.; Guldi, D. M.; Peukert, W.; Hartmann, M.; Meyer, K.; Schmuki, P. Noble-metal-free Photocatalytic Hydrogen Evolution Activity: The Impact of Ball Milling Anatase Nanopowders with TiH_2. *Adv. Mater.* **2017**, *29*, 1604747.
(39) Liu, N.; Häublein, V.; Zhou, X.; Venkatesan, U.; Hartmann, M.; Mačković, M.; Nakajima, T.; Spiecker, E.; Osvet, A.; Frey, L.; Schmuki, P. Black" TiO_2 Nanotubes Formed by High-energy Proton Implantation Show Noble-metal-*co*-catalyst Free Photocatalytic H_2-Evolution. *Nano Lett.* **2015**, *15*, 6815−6820.
(40) Zhou, X.; Zolnhofer, E. M.; Nguyen, N. T.; Liu, N.; Meyer, K.; Schmuki, P. Stable Co-catalyst-free Photocatalytic H_2 Evolution From Oxidized Titanium Nitride Nanopowders. *Angew. Chem., Int. Ed.* **2015**, *54*, 13385−13389.
(41) Cui, H.; Zhao, W.; Yang, C.; Yin, H.; Lin, T.; Shan, Y.; Xie, Y.; Gu, H.; Huang, F. Black TiO_2 Nanotube Arrays for High-efficiency Photoelectrochemical Water-splitting. *J. Mater. Chem. A* **2014**, *2*, 8612−8616.
(42) Zhou, X.; Liu, N.; Schmuki, P. Photocatalysis with TiO_2 Nanotubes: "Colorful" Reactivity and Designing Site-specific Photocatalytic Centers into TiO_2 Nanotubes. *ACS Catal.* **2017**, *7*, 3210−3235.
(43) Xu, J.; Tian, Z.; Yin, G.; Lin, T.; Huang, F. Controllable Reduced Black Titania with Enhanced Photoelectrochemical Water Splitting Performance. *Dalton Trans* **2017**, *46*, 1047−1051.
(44) Mascaretti, L.; Ferrulli, S.; Mazzolini, P.; Casari, C. S.; Russo, V.; Matarrese, R.; Nova, I.; Terraneo, G.; Liu, N.; Schmuki, P.; Li Bassi, A. Hydrogen-treated Hierarchical Titanium Oxide Nanostructures for Photoelectrochemical Water Splitting. *Sol. Energy Mater. Sol. Cells* **2017**, *169*, 19−27.
(45) Cho, I. S.; Logar, M.; Lee, C. H.; Cai, L.; Prinz, F. B.; Zheng, X. Rapid and Controllable Flame Reduction of TiO_2 Nanowires for Enhanced Solar Water-splitting. *Nano Lett.* **2014**, *14*, 24−31.
(46) Wang, G.; Wang, H.; Ling, Y.; Tang, Y.; Yang, X.; Fitzmorris, R. C.; Wang, C.; Zhang, J. Z.; Li, Y. Hydrogen-treated TiO_2 Nanowire Arrays for Photoelectrochemical Water Splitting. *Nano Lett.* **2011**, *11*, 3026−3033.
(47) Zhu, G.; Yin, H.; Yang, C.; Cui, H.; Wang, Z.; Xu, J.; Lin, T.; Huang, F. Black Titania for Superior Photocatalytic Hydrogen Production and Photoelectrochemical Water Splitting. *ChemCatChem* **2015**, *7*, 2614−2619.
(48) Nakajima, T.; Nakamura, T.; Shinoda, K.; Tsuchiya, T. Rapid Formation of Black Titania Photoanodes: Pulsed Laser-induced Oxygen Release and Enhanced Solar Water Splitting Efficiency. *J. Mater. Chem. A* **2014**, *2*, 6762−6771.
(49) Wang, Z.; Yang, C.; Lin, T.; Yin, H.; Chen, P.; Wan, D.; Xu, F.; Huang, F.; Lin, J.; Xie, X.; Jiang, M. Visible-light Photocatalytic, Solar

DOI: 10.1021/acscatal.8b04068
ACS Catal. 2019, 9, 345−364

Thermal and Photoelectrochemical Properties of Aluminium-reduced Black Titania. *Energy Environ. Sci.* **2013**, *6*, 3007−3014.
(50) Mohajernia, S.; Hejazi, S.; Mazare, A.; Nguyen, N. T.; Schmuki, P. Photoelectrochemical H_2 Generation from Suboxide TiO_2 Nanotubes: Visible-light Absorption versus Conductivity. *Chem. - Eur. J.* **2017**, *23*, 12406−12411.
(51) Zhang, K.; Ravishankar, S.; Ma, M.; Veerappan, G.; Bisquert, J.; Fabregat-Santiago, F.; Park, J. H. Overcoming Charge Collection Limitation at Solid/Liquid Interface by a Controllable Crystal Deficient Overlayer. *Adv. Energy Mater.* **2017**, *7*, 1600923.
(52) Zhang, K.; Park, J. H. Surface Localization of Defects in Black TiO_2: Enhancing Photoactivity or Reactivity. *J. Phys. Chem. Lett.* **2017**, *8*, 199−207.
(53) Li, G.; Blake, G. R.; Palstra, T. T. M. Vacancies in Functional Materials for Clean Energy Storage and Harvesting: The Perfect Imperfection. *Chem. Soc. Rev.* **2017**, *46*, 1693−1706.
(54) Paul, A.; Laurila, T.; Vuorinen, V.; Divinski, S. V. *Thermodynamics, Diffusion and the Kirkendall Effect in Solids*; Springer International Publishing Switzerland: Basel, Switzerland, 2014; p 530.
(55) Callister, W. D., Jr.; Rethwisch, D. G. *Materials Science and Engineering: An Introduction*, 9th ed.; John Wiley and Sons, Inc.: Hoboken, NJ, 2013; p 992.
(56) Naldoni, A.; Allieta, M.; Santangelo, S.; Marelli, M.; Fabbri, F.; Cappelli, S.; Bianchi, C. L.; Psaro, R.; Dal Santo, V. Effect of Nature and Location of Defects on Bandgap Narrowing in Black TiO_2 Nanoparticles. *J. Am. Chem. Soc.* **2012**, *134*, 7600−7603.
(57) Chen, X.; Burda, C. The Electronic Origin of the Visible-light Absorption Properties of C-, N- and S-doped TiO_2 Nanomaterials. *J. Am. Chem. Soc.* **2008**, *130*, 5018−5019.
(58) Naldoni, A.; Fabbri, F.; Altomare, M.; Marelli, M.; Psaro, R.; Selli, E.; Salviati, G.; Dal Santo, V. The Critical Role of Intragap States in the Energy Transfer from Gold Nanoparticles to TiO_2. *Phys. Chem. Chem. Phys.* **2015**, *17*, 4864−4869.
(59) Yang, H. G.; Sun, C. H.; Qiao, S. Z.; Zou, J.; Liu, G.; Smith, S. C.; Cheng, H. M.; Lu, G. Q. Anatase TiO_2 Single Crystals with a Large Percentage of Reactive Facets. *Nature* **2008**, *453*, 638−641.
(60) Penn, R. L.; Banfield, J. F. Formation of Rutile Nuclei at Anatase {112} Twin Interfaces and the Phase Transformation Mechanism in Nanocrystalline Titania. *Am. Mineral.* **1999**, *84*, 871−876.
(61) Esch, F.; Fabris, S.; Zhou, L.; Montini, T.; Africh, C.; Fornasiero, P.; Comelli, G.; Rosei, R. Electron Localization Determines Defect Formation on Ceria Substrates. *Science* **2005**, *309*, 752−755.
(62) Campbell, C. T.; Peden, C. H. F. Oxygen Vacancies and Catalysis on Ceria Surfaces. *Science* **2005**, *309*, 713−714.
(63) Cordero, F. Hopping and Clustering of Oxygen Vacancies in $SrTiO_3$ by Anelastic Relaxation. *Phys. Rev. B: Condens. Matter Mater. Phys.* **2007**, *76*, 172106.
(64) Eom, K.; Choi, E.; Choi, M.; Han, S.; Zhou, H.; Lee, J. Oxygen Vacancy Linear Clustering in a Perovskite Oxide. *J. Phys. Chem. Lett.* **2017**, *8*, 3500−3505.
(65) Uberuaga, B. P.; Pilania, G. Effect of Cation Ordering on Oxygen Vacancy Diffusion Pathways in Double Perovskites. *Chem. Mater.* **2015**, *27*, 5020−5026.
(66) Viola, M. C.; Martínez-Lope, M. J.; Alonso, J. A.; Velasco, P.; Martínez, J. L.; Pedregosa, J. C.; Carbonio, R. E.; Fernández-Díaz, M. T. Induction of Colossal Magnetoresistance in the Double Perovskite Sr_2CoMoO_6. *Chem. Mater.* **2002**, *14*, 812−818.
(67) Pavlenko, N.; Kopp, T.; Tsymbal, E. Y.; Mannhart, J.; Sawatzky, G. A. Oxygen Vacancies at Titanate Interfaces: Two-dimensional Magnetism and Orbital Reconstruction. *Phys. Rev. B: Condens. Matter Mater. Phys.* **2012**, *86*, 064431.
(68) He, Y.; Dulub, O.; Cheng, H.; Selloni, A.; Diebold, U. Evidence for the Predominance of Subsurface Defects on Reduced Anatase TiO_2(101). *Phys. Rev. Lett.* **2009**, *102*, 106105.
(69) Sekiya, T.; Takeda, H.; Kamiya, N.; Kurita, S.; Kodaira, T. EPR of Anatase Titanium Dioxide under UV Light Irradiation. *Phys. Status Solidi C* **2006**, *3*, 3603−3606.
(70) Chester, P. F. Electron Spin Resonance in Semiconducting Rutile. *J. Appl. Phys.* **1961**, *32*, 2233−2236.
(71) Aono, M.; Hasiguti, R. R. Interaction and Ordering of Lattice Defects in Oxygen-deficient Rutile TiO_{2-x}. *Phys. Rev. B: Condens. Matter Mater. Phys.* **1993**, *48*, 12406−12414.
(72) Hasiguti, R. R.; Yagi, E.; Aono, M. Electrical Conductivity of Slightly Reduced Rutile between 2 and 370 K. *Radiat. Eff.* **1970**, *4*, 137−140.
(73) Chiesa, M.; Livraghi, S.; Giamello, E.; Albanese, E.; Pacchioni, G. Ferromagnetic Interactions in Highly Stable, Partially Reduced TiO_2: The S = 2 State in Anatase. *Angew. Chem., Int. Ed.* **2017**, *56*, 2604−2607.
(74) Brant, A. T.; Golden, E. M.; Giles, N. C.; Yang, S.; Sarker, M. A. R.; Watauchi, S.; Nagao, M.; Tanaka, I.; Tryk, D. A.; Manivannan, A.; Halliburton, L. E. Triplet Ground State of the Neutral Oxygen-vacancy Donor in Rutile TiO_2. *Phys. Rev. B: Condens. Matter Mater. Phys.* **2014**, *89*, 115206.
(75) Chiesa, M.; Paganini, M. C.; Livraghi, S.; Giamello, E. Charge Trapping in TiO_2 Polymorphs as Seen by Electron Paramagnetic Resonance Spectroscopy. *Phys. Chem. Chem. Phys.* **2013**, *15*, 9435−9447.
(76) Livraghi, S.; Chiesa, M.; Paganini, M. C.; Giamello, E. On the Nature of Reduced States in Titanium Dioxide as Monitored by Electron Paramagnetic Resonance. I: The Anatase Case. *J. Phys. Chem. C* **2011**, *115*, 25413−25421.
(77) Sun, Y.; Egawa, T.; Shao, C.; Zhang, L.; Yao, X. Quantitative Study of F Center in High-surface-area Anatase Titania Nanoparticles Prepared by MOCVD. *J. Phys. Chem. Solids* **2004**, *65*, 1793−1797.
(78) Nakamura, I.; Negishi, N.; Kutsuna, S.; Ihara, T.; Sugihara, S.; Takeuchi, K. Role of Oxygen Vacancy in the Plasma-treated TiO_2 Photocatalyst with Visible Light Activity for NO Removal. *J. Mol. Catal. A: Chem.* **2000**, *161*, 205−212.
(79) Misra, S. K.; Andronenko, S. I.; Tipikin, D.; Freed, J. H.; Somani, V.; Prakash, O. Study of Paramagnetic Defect Centers in As-grown and Annealed TiO_2 Anatase and Rutile Nanoparticles by a Variable-temperature X-band and High-frequency (236 GHz) EPR. *J. Magn. Magn. Mater.* **2016**, *401*, 495−505.
(80) Baumann, S. O.; Elser, M. J.; Auer, M.; Bernardi, J.; Hüsing, N.; Diwald, O. Solid−Solid Interface Formation in TiO_2 Nanoparticle Networks. *Langmuir* **2011**, *27*, 1946−1953.
(81) Minnekhanov, A. A.; Deygen, D. M.; Konstantinova, E. A.; Vorontsov, A. S.; Kashkarov, P. K. Paramagnetic Properties of Carbon-doped Titanium Dioxide. *Nanoscale Res. Lett.* **2012**, *7*, 333.
(82) Kuznetsov, V. N.; Serpone, N. On the Origin of the Spectral Bands in the Visible Absorption Spectra of Visible-light-active TiO_2 Specimens Analysis and Assignments. *J. Phys. Chem. C* **2009**, *113*, 15110−15123.
(83) Panarelli, E. G.; Livraghi, S.; Maurelli, S.; Polliotto, V.; Chiesa, M.; Giamello, E. Role of Surface Water Molecules in Stabilizing Trapped Hole Centres in Titanium Dioxide (Anatase) as Monitored by Electron Paramagnetic Resonance. *J. Photochem. Photobiol., A* **2016**, *322*−*323*, 27−34.
(84) Kumar, C. P.; Gopal, N. O.; Wang, T. C.; Wong, M.-S.; Ke, S. C. EPR Investigation of TiO_2 Nanoparticles with Temperature-dependent Properties. *J. Phys. Chem. B* **2006**, *110*, 5223−5229.
(85) Yang, S.; Brant, A. T.; Halliburton, L. E. Photoinduced Self-trapped Hole Center in TiO_2 Crystals. *Phys. Rev. B: Condens. Matter Mater. Phys.* **2010**, *82*, 035209.
(86) Grunin, V. S.; Davtyan, G. D.; Ioffe, V. A.; Patrina, I. B. EPR of Cu^{2+} and Radiation Centres in Anatase (TiO_2). *Phys. Status Solidi B* **1976**, *77*, 85−92.
(87) Carter, E.; Carley, A. F.; Murphy, D. M. Evidence for O_2^- Radical Stabilization at Surface Oxygen Vacancies on Polycrystalline TiO_2. *J. Phys. Chem. C* **2007**, *111*, 10630−10638.
(88) Hurum, D. C.; Agrios, A. G.; Gray, K. A.; Rajh, T.; Thurnauer, M. C. Explaining the Enhanced Photocatalytic Activity of Degussa P25 Mixed-Phase TiO_2 Using EPR. *J. Phys. Chem. B* **2003**, *107*, 4545−4549.

DOI: 10.1021/acscatal.8b04068
ACS Catal. 2019, 9, 345−364

(89) Coronado, J. M.; Maira, A. J.; Conesa, J. C.; Yeung, K. L.; Augugliaro, V.; Soria, J. EPR Study of the Surface Characteristics of Nanostructured TiO_2 under UV Irradiation. *Langmuir* **2001**, *17*, 5368−5374.
(90) López-Muñoz, M. J.; Soria, J.; Conesa, J. C.; Augugliaro, V. ESR Study of Photo-oxidation of Phenol at Low Temperature on Polycrystalline Titanium Dioxide. *Stud. Surf. Sci. Catal.* **1994**, *82*, 693−701.
(91) McCain, D. C.; Palke, W. E. Theory of Electron Spin *g*-values for Peroxy Radicals. *J. Magn. Reson. (1969-1992)* **1975**, *20*, 52−66.
(92) Chen, X.; Liu, L.; Huang, F. Black Titanium Dioxide (TiO_2) Nanomaterials. *Chem. Soc. Rev.* **2015**, *44*, 1861−1885.
(93) Wajid Shah, M.; Zhu, Y.; Fan, X.; Zhao, J.; Li, Y.; Asim, S.; Wang, C. Facile Synthesis of Defective TiO_{2-x} Nanocrystals with High Surface Area and Tailoring Bandgap for Visible-light Photocatalysis. *Sci. Rep.* **2015**, *5*, 15804.
(94) Montoya, A. T.; Gillan, E. G. Enhanced Photocatalytic Hydrogen Evolution from Transition-metal Surface-modified TiO_2. *ACS Omega* **2018**, *3*, 2947−2955.
(95) Cushing, S. K.; Meng, F.; Zhang, J.; Ding, B.; Chen, C. K.; Chen, C.-J.; Liu, R.-S.; Bristow, A. D.; Bright, J.; Zheng, P.; Wu, N. Effects of Defects on Photocatalytic Activity of Hydrogen-treated Titanium Oxide Nanobelts. *ACS Catal.* **2017**, *7*, 1742−1748.
(96) Henderson, M. A.; Lyubinetsky, I. Molecular-level Insights into Photocatalysis from Scanning Probe Microscopy Studies on TiO_2(110). *Chem. Rev.* **2013**, *113*, 4428−4455.
(97) Vohs, J. M. Site Requirements for the Adsorption and Reaction of Oxygenates on Metal Oxide Surfaces. *Chem. Rev.* **2013**, *113*, 4136−4163.
(98) Guo, Q.; Zhou, C.; Ma, Z.; Ren, Z.; Fan, H.; Yang, X. Elementary Photocatalytic Chemistry on TiO_2 Surfaces. *Chem. Soc. Rev.* **2016**, *45*, 3701−3730.
(99) Li, H.; Guo, Y.; Robertson, J. Calculation of TiO_2 Surface and Subsurface Oxygen Vacancy by the Screened Exchange Functional. *J. Phys. Chem. C* **2015**, *119*, 18160−18166.
(100) Malashevich, A.; Jain, M.; Louie, S. G. First-principles DFT + *GW* Study of Oxygen Vacancies in Rutile TiO_2. *Phys. Rev. B: Condens. Matter Mater. Phys.* **2014**, *89*, 075205.
(101) Mattioli, G.; Filippone, F.; Alippi, P.; Amore Bonapasta, A. *Ab Initio* Study of the Electronic States Induced by Oxygen Vacancies in Rutile and Anatase TiO_2. *Phys. Rev. B: Condens. Matter Mater. Phys.* **2008**, *78*, 241201.
(102) Livraghi, S.; Maurelli, S.; Paganini, M. C.; Chiesa, M.; Giamello, E. Probing the Local Environment of Ti^{3+} Ions in TiO_2 (Rutile) by ^{17}O HYSCORE. *Angew. Chem., Int. Ed.* **2011**, *50*, 8038−8040.
(103) Maurelli, S.; Livraghi, S.; Chiesa, M.; Giamello, E.; Van Doorslaer, S.; Di Valentin, C.; Pacchioni, G. Hydration Structure of the Ti(III) Cation as Revealed by Pulse EPR and DFT Studies: New Insights into a Textbook Case. *Inorg. Chem.* **2011**, *50*, 2385−2394.
(104) Bilmes, S. A.; Mandelbaum, P.; Alvarez, F.; Victoria, N. M. Surface and Electronic Structure of Titanium Dioxide Photocatalysts. *J. Phys. Chem. B* **2000**, *104*, 9851−9858.
(105) Justicia, I.; Ordejón, P.; Canto, G.; Mozos, J. L.; Fraxedas, J.; Battiston, G. A.; Gerbasi, R.; Figueras, A. Designed Self-doped Titanium Oxide Thin Films for Efficient Visible-light Photocatalysis. *Adv. Mater.* **2002**, *14*, 1399−1402.
(106) Wendt, S.; Sprunger, P. T.; Lira, E.; Madsen, G. K. H.; Li, Z.; Hansen, J. Ø.; Matthiesen, J.; Blekinge-Rasmussen, A.; Lægsgaard, E.; Hammer, B.; Besenbacher, F. The Role of Interstitial Sites in the Ti3*d* Defect State in the Band Gap of Titania. *Science* **2008**, *320*, 1755−1759.
(107) He, Y.; Tilocca, A.; Dulub, O.; Selloni, A.; Diebold, U. Local Ordering and Electronic Signatures of Submonolayer Water on Anatase TiO_2(101). *Nat. Mater.* **2009**, *8*, 585−589.
(108) Lira, E.; Wendt, S.; Huo, P.; Hansen, J. Ø.; Streber, R.; Porsgaard, S.; Wei, Y.; Bechstein, R.; Lægsgaard, E.; Besenbacher, F. The Importance of Bulk Ti^{3+} Defects in the Oxygen Chemistry on Titania Surfaces. *J. Am. Chem. Soc.* **2011**, *133*, 6529−6532.
(109) Gong, X.-Q.; Selloni, A.; Batzill, M.; Diebold, U. Steps on Anatase TiO_2(101). *Nat. Mater.* **2006**, *5*, 665−670.
(110) Li, J.; Lazzari, R.; Chenot, S.; Jupille, J. Contributions of Oxygen Vacancies and Titanium Interstitials to Band-gap States of Reduced Titania. *Phys. Rev. B: Condens. Matter Mater. Phys.* **2018**, *97*, 041403.
(111) Huygh, S.; Bogaerts, A.; Neyts, E. C. How Oxygen Vacancies Activate CO_2 Dissociation on TiO_2 Anatase (001). *J. Phys. Chem. C* **2016**, *120*, 21659−21669.
(112) Lang, X.; Liang, Y.; Sun, L.; Zhou, S.; Lau, W.-M. Interplay between Methanol and Anatase TiO_2(101) Surface: The Effect of Subsurface Oxygen Vacancy. *J. Phys. Chem. C* **2017**, *121*, 6072−6080.
(113) Martinez, U.; Hansen, J. Ø.; Lira, E.; Kristoffersen, H. H.; Huo, P.; Bechstein, R.; Lægsgaard, E.; Besenbacher, F.; Hammer, B.; Wendt, S. Reduced Step Edges on Rutile TiO_2(110) as Competing Defects to Oxygen Vacancies on the Terraces and Reactive Sites for Ethanol Dissociation. *Phys. Rev. Lett.* **2012**, *109*, 155501.
(114) Guo, Q.; Xu, C.; Ren, Z.; Yang, W.; Ma, Z.; Dai, D.; Fan, H.; Minton, T. K.; Yang, X. Stepwise Photocatalytic Dissociation of Methanol and Water on TiO_2(110). *J. Am. Chem. Soc.* **2012**, *134*, 13366−13373.
(115) Zhou, C.; Ren, Z.; Tan, S.; Ma, Z.; Mao, X.; Dai, D.; Fan, H.; Yang, X.; LaRue, J.; Cooper, R.; Wodtke, A. M.; Wang, Z.; Li, Z.; Wang, B.; Yang, J.; Hou, J. Site-specific Photocatalytic Splitting of Methanol on TiO_2(110). *Chem. Sci.* **2010**, *1*, 575−580.
(116) Liu, L.; Yu, P. Y.; Chen, X.; Mao, S. S.; Shen, D. Z. Hydrogenation and Disorder in Engineered Black TiO_2. *Phys. Rev. Lett.* **2013**, *111*, 065505.
(117) Xia, T.; Chen, X. Revealing the Structural Properties of Hydrogenated Black TiO_2 Nanocrystals. *J. Mater. Chem. A* **2013**, *1*, 2983−2989.
(118) Zheng, Z.; Huang, B.; Lu, J.; Wang, Z.; Qin, X.; Zhang, X.; Dai, Y.; Whangbo, M.-H. Hydrogenated Titania: Synergy of Surface Modification and Morphology Improvement for Enhanced Photocatalytic Activity. *Chem. Commun.* **2012**, *48*, 5733−5735.
(119) Zhu, Y.; Liu, D.; Meng, M. H_2 Spillover Enhanced Hydrogenation Capability of TiO_2 Used for Photocatalytic Splitting of Water: a Traditional Phenomenon for New Applications. *Chem. Commun.* **2014**, *50*, 6049−6051.
(120) Zuo, F.; Wang, L.; Wu, T.; Zhang, Z.; Borchardt, D.; Feng, P. Self-doped Ti^{3+} Enhanced Photocatalyst for Hydrogen Production under Visible Light. *J. Am. Chem. Soc.* **2010**, *132*, 11856−11857.
(121) Yang, C.; Wang, Z.; Lin, T.; Yin, H.; Lü, X.; Wan, D.; Xu, T.; Zheng, C.; Lin, J.; Huang, F.; Xie, X.; Jiang, M. Core-shell Nanostructured "Black" Rutile Titania as Excellent Catalyst for Hydrogen Production Enhanced by Sulfur Doping. *J. Am. Chem. Soc.* **2013**, *135*, 17831−17838.
(122) Sinhamahapatra, A.; Jeon, J.-P.; Yu, J.-S. A New Approach to Prepare Highly Active and Stable Black Titania for Visible Light-assisted Hydrogen Production. *Energy Environ. Sci.* **2015**, *8*, 3539−3544.
(123) Zanella, R.; Giorgio, S.; Henry, C. R.; Louis, C. Alternative Methods for the Preparation of Gold Nanoparticles Supported on TiO_2. *J. Phys. Chem. B* **2002**, *106*, 7634−7642.
(124) Corma, A.; Garcia, H. Supported Gold Nanoparticles as Catalysts for Organic Reactions. *Chem. Soc. Rev.* **2008**, *37*, 2096−2126.
(125) Cushing, B. L.; Kolesnichenko, V. L.; O'Connor, C. J. Recent Advances in the Liquid-phase Syntheses of Inorganic Nanoparticles. *Chem. Rev.* **2004**, *104*, 3893−3946.
(126) Zhu, Y.; Liu, D.; Meng, M. H_2 Spillover Enhanced Hydrogenation Capability of TiO_2 Used for Photocatalytic Splitting of Water: A Traditional Phenomenon for New Applications. *Chem. Commun.* **2014**, *50*, 6049−6051.
(127) Liu, N.; Schneider, C.; Freitag, D.; Zolnhofer, E. M.; Meyer, K.; Schmuki, P. Noble-metal-free Photocatalytic H_2 Generation: Active and Inactive 'Black' TiO_2 Nanotubes and Synergistic Effects. *Chem. - Eur. J.* **2016**, *22*, 13810−13814.

DOI: 10.1021/acscatal.8b04068
ACS Catal. 2019, 9, 345−364

(128) Kong, M.; Li, Y.; Chen, X.; Tian, T.; Fang, P.; Zheng, F.; Zhao, X. Tuning the Relative Concentration Ratio of Bulk Defects to Surface Defects in TiO_2 Nanocrystals Leads to High Photocatalytic Efficiency. *J. Am. Chem. Soc.* **2011**, *133*, 16414−16417.
(129) Cronemeyer, D. C. Infrared Absorption of Reduced Rutile TiO_2 Single Crystals. *Phys. Rev.* **1959**, *113*, 1222−1226.
(130) Xue, J.; Zhu, X.; Zhang, Y.; Wang, W.; Xie, W.; Zhou, J.; Bao, J.; Luo, Y.; Gao, X.; Wang, Y.; Jang, L.-y.; Sun, S.; Gao, C. Nature of Conduction Band Tailing in Hydrogenated Titanium Dioxide for Photocatalytic Hydrogen Evolution. *ChemCatChem* **2016**, *8*, 2010−2014.
(131) Zhang, X.; Hu, W.; Zhang, K.; Wang, J.; Sun, B.; Li, H.; Qiao, P.; Wang, L.; Zhou, W. Ti^{3+} Self-Doped Black TiO_2 Nanotubes with Mesoporous Nanosheet Architecture as Efficient Solar-driven Hydrogen Evolution Photocatalysts. *ACS Sustainable Chem. Eng.* **2017**, *5*, 6894−6901.
(132) Pore, V.; Ritala, M.; Leskelä, M.; Areva, S.; Järn, M.; Järnström, J. H_2S Modified Atomic Layer Deposition Process for Photocatalytic TiO_2 Thin Films. *J. Mater. Chem.* **2007**, *17*, 1361−1371.
(133) Prokes, S. M.; Gole, J. L.; Chen, X.; Burda, C.; Carlos, W. E. Defect-related Optical Behavior in Surface Modified TiO_2 Nanostructures. *Adv. Funct. Mater.* **2005**, *15*, 161−167.
(134) Kroll, W. The Production of Ductile Titanium. *Trans. Electrochem. Soc.* **1940**, *78*, 35−47.
(135) Bamwenda, G. R.; Tsubota, S.; Kobayashi, T.; Haruta, M. Photoinduced Hydrogen Production from an Aqueous Solution of Ethylene Glycol over Ultrafine Gold Supported on TiO_2. *J. Photochem. Photobiol., A* **1994**, *77*, 59−67.
(136) Bamwenda, G. R.; Tsubota, S.; Nakamura, T.; Haruta, M. Photoassisted Hydrogen Production from a Water-ethanol Solution: A Comparison of Activities of Au−TiO_2 and Pt−TiO_2. *J. Photochem. Photobiol., A* **1995**, *89*, 177−189.
(137) Spanu, D.; Recchia, S.; Mohajernia, S.; Tomanec, O.; Kment, Š.; Zboril, R.; Schmuki, P.; Altomare, M. Templated Dewetting−Alloying of NiCu Bilayers on TiO_2 Nanotubes Enables Efficient Noble Metal-free Photocatalytic H_2 Evolution. *ACS Catal.* **2018**, *8*, 5298−5305.
(138) Naldoni, A.; D'Arienzo, M.; Altomare, M.; Marelli, M.; Scotti, R.; Morazzoni, F.; Selli, E.; Dal Santo, V. Pt and Au/TiO_2 Photocatalysts for Methanol Reforming: Role of Metal Nanoparticles in Tuning Charge Trapping Properties and Photoefficiency. *Appl. Catal., B* **2013**, *130−131*, 239−248.
(139) Liu, N.; Schneider, C.; Freitag, D.; Hartmann, M.; Venkatesan, U.; Müller, J.; Spiecker, E.; Schmuki, P. Black TiO_2 Nanotubes: Cocatalyst-free Open-circuit Hydrogen Generation. *Nano Lett.* **2014**, *14*, 3309−3313.
(140) Liu, N.; Steinrück, H.-G.; Osvet, A.; Yang, Y.; Schmuki, P. Noble Metal Free Photocatalytic H_2 Generation on Black TiO_2: On the Influence of Crystal Facets vs. Crystal Damage. *Appl. Phys. Lett.* **2017**, *110*, 072102.
(141) Abbaschian, R.; Reed-Hill, R. E. *Physical Metallurgy Principles*; Cengage Learning: Boston, MA, 2010; p 750.
(142) Makin, M. J. *The Nature of Small Defect Clusters*: Report of a Consultants Symposium Held at A. E. R. E., Harwell, on July 4−6th, 1966; H.M. Stationery Office: London, 1966; p 592.
(143) Wei, L. H.; Wu, S. Y.; Zhang, Z. H.; Wang, X. F.; Hu, Y. X. Investigations on the Local Structure and *g* Factors for the Interstitial Ti^{3+} in TiO_2. *Pramana* **2008**, *71*, 167−173.
(144) Kumar, C. P.; Gopal, N. O.; Wang, T. C.; Wong, M.-S.; Ke, S. C. EPR Investigation of TiO_2 Nanoparticles with Temperature-dependent Properties. *J. Phys. Chem. B* **2006**, *110*, 5223−5229.
(145) Pan, X.; Yang, M.-Q.; Fu, X.; Zhang, N.; Xu, Y.-J. Defective TiO_2 with Oxygen Vacancies: Synthesis, Properties and Photocatalytic Applications. *Nanoscale* **2013**, *5*, 3601−3614.
(146) Brückner, A. *In Situ* Electron Paramagnetic Resonance: A Unique Tool for Analyzing Structure−reactivity Relationships in Heterogeneous Catalysis. *Chem. Soc. Rev.* **2010**, *39*, 4673−4684.
(147) Deskins, N. A.; Rousseau, R.; Dupuis, M. Distribution of Ti^{3+} Surface Sites in Reduced TiO_2. *J. Phys. Chem. C* **2011**, *115*, 7562−7572.
(148) Justicia, I.; Ordejón, P.; Canto, G.; Mozos, J. L.; Fraxedas, J.; Battiston, G. A.; Gerbasi, R.; Figueras, A. Designed Self-doped Titanium Oxide Thin Films for Efficient Visible-light Photocatalysis. *Adv. Mater.* **2002**, *14*, 1399−1402.
(149) Zhou, X.; Liu, N.; Schmuki, P. Ar^+-ion Bombardment of TiO_2 Nanotubes Creates Co-catalytic Effect for Photocatalytic Open Circuit Hydrogen Evolution. *Electrochem. Commun.* **2014**, *49*, 60−64.
(150) AlSalka, Y.; Hakki, A.; Schneider, J.; Bahnemann, D. W. Co-catalyst-free Photocatalytic Hydrogen Evolution on TiO_2: Synthesis of Optimized Photocatalyst through Statistical Material Science. *Appl. Catal., B* **2018**, *238*, 422−433.
(151) Zhou, X.; Häublein, V.; Liu, N.; Nguyen, N. T.; Zolnhofer, E. M.; Tsuchiya, H.; Killian, M. S.; Meyer, K.; Frey, L.; Schmuki, P. TiO_2 Nanotubes: Nitrogen-ion Implantation at Low Dose Provides Noble-metal-free Photocatalytic H_2-evolution Activity. *Angew. Chem., Int. Ed.* **2016**, *55*, 3763−3767.
(152) Scanlon, D. O.; Dunnill, C. W.; Buckeridge, J.; Shevlin, S. A.; Logsdail, A. J.; Woodley, S. M.; Catlow, C. R. A.; Powell, M. J.; Palgrave, R. G.; Parkin, I. P.; Watson, G. W.; Keal, T. W.; Sherwood, P.; Walsh, A.; Sokol, A. A. Band Alignment of Rutile and Anatase TiO_2. *Nat. Mater.* **2013**, *12*, 798−801.
(153) Hernández, S.; Hidalgo, D.; Sacco, A.; Chiodoni, A.; Lamberti, A.; Cauda, V.; Tresso, E.; Saracco, G. Comparison of Photocatalytic and Transport Properties of TiO_2 and ZnO Nanostructures for Solar-driven Water Splitting. *Phys. Chem. Chem. Phys.* **2015**, *17*, 7775−7786.

DOI: 10.1021/acscatal.8b04068
ACS Catal. 2019, 9, 345−364